FORSCHUNGSZENTRUM
ROSSENDORF e.V.

FZR

FZR-158
November 1996

W. Matz, F. Prokert, R. Schlenk, J. Claußner,
N. Schell, F. Eichhorn and G. Bernhard

The Rossendorf Beamline at the ESRF (Project ROBL)

Forschungszentrum Rossendorf e.V.
Postfach 51 01 19 · D-01314 Dresden
Bundesrepublik Deutschland

Telefon **(0351) 260 3122**
Telefax **(0351) 260 3438**
E-Mail **matz@fz-rossendorf.de**

The Rossendorf Beamline at the ESRF (Project ROBL)

Part 1: Beamline Design

W. Matz, F. Prokert, R. Schlenk, J. Claußner, N. Schell, F. Eichhorn, G. Bernhard

Abstract

In this final design report the general layout and the optics of the beamline ROBL is described. The beamline is buildt by the Research Center Rossendorf at the bending magnet source BM20 of the European Synchrotron Radiation Facility (ESRF), Grenoble. The design criteria for the beamline optics and the adopted solutions are reported in detail. Some performance data of the beamline as resolution, focussing and intensity are modelled by the ray-tracing code SHADOW. Furthermore the layout of the vacuum system is described.

Zusammenfassung

In diesem abschließenden Entwurfsbericht für das Strahlrohrprojekt ROBL werden die Gesamtstruktur und die Röntgenoptik beschrieben. Das Forschungszentrum Rossendorf errichtet dieses Strahlrohr am Ablenkmagneten BM20 der Europäischen Synchrotronstrahlungsquelle (ESRF) in Grenoble. Die Entwurfskriterien für die Röntgenoptik und die ausgewählten Lösungen werden detailliert dargestellt. Die für den Experimentator wesentlichen Parameter we Auflösung, Fokussierung und Intensität wurden z.T. analytisch berechnet oder mit dem Programm SHADOW modelliert. Das Vakuumsystem wird ebenfalls beschrieben.

Contents

1. Introduction

The Research Center Rossendorf Inc. (Forschungszentrum Rossendorf e.V. - FZR) has established a Collaborating Research Group (CRG) at the European Synchrotron Radiation Facility (ESRF) The aim of this CRG is to construct and run a beamline at a bending magnet of the ESRF for investigations in radiochemistry and materials science. The project is named ROBL (*RO*ssendorf *B*eam*L*ine).

The Research Center Rossendorf Inc. near Dresden was founded in the beginning of 1992 according to recommendations of the German Science Council. It is the scientific successor organisation of the Central Institute of Nuclear Research (CINR). The Research Center Rossendorf is run by the State of Saxony and the budget is shared in equal parts between Saxony and the Federal Government of Germany.

The research activities of the FZR are distributed in the five institutes of Ion Beam Physics and Materials Research,
Bioinorganic and Radiopharmaceutical Chemistry,
Radiochemistry,
Nuclear and Hadron Physics,
Safety Research.
The scientific programs of the institutes have their roots in the former CINR but received a new structure and additional goals in the 1992/93 period of determining the profile of the FZR as a whole. In different parts of the program, the use of synchrotron radiation techniques will play an important role in the future.

At the FZR, mainly the Institute of Radiochemistry as well as the Institute of Ion Beam Physics and Materials Research are interested in synchrotron radiation. Both institutes are developing collaborations with research groups at universities and institutes in Saxony and worldwide which are particularly interested in the use of synchrotron radiation. Moreover, as a fully state funded research organisation the FZR will make available its sophisticated equipment partly to universities and other research groups.
Thus, the aims of the realisation of the ROBL project under the responsibility of the FZR are twofold: It will allow dedicated investigations which are essential parts of the research programs of the institutes of the FZR and it will provide a sophisticated facility accessible for external research groups, in particular from the regional research community.

For the Institute of Radiochemistry at the FZR, there is an indispensable need for synchrotron X-ray absorption spectroscopy (XAS) for chemical investigations on actinide or other radioactive materials mainly from the point of view of radioecology. The Institute of Ion Beam Physics and Materials Research proposes investigations of the formation and structure of thin films and buried layers produced by ion beam methods. Therefore the beam line will comprise

- a XAS experimental station for the investigation of solid and liquid samples of radioactive materials and/or micro beam scanning techniques and

- an experimental station for materials science, particularly for the study of surface layers and thin films by X-ray techniques.

The XAS end station for radioactive materials would be nearly unique in the world, only at the Stanford Synchrotron Radiation Laboratory similar facilities exist, but not with the outstanding beam quality as supplied by the ESRF. The conditions of the "Zone Contrôlée" at the site of ESRF and ILL in Grenoble are appropriate for the investigation of radioactive samples.

The two experimental end stations are located behind each other and will be used alternatively. The design of ROBL is constrained by considerations of space, of safety aspects for handling low activity samples as well as the intensity and divergence of the bending magnet radiation. Nevertheless, the projected specifications will exceed those available on second generation synchrotron sources. Further, there will be a dedicated equipment for the investigation of radioactive samples up to an activity limit of 185 MBq.

The FZR and its partners will use most of the beam time available. According to the conditions of the ESRF, one third of the beam time will be made available for general users with the provision that not all of the special equipment can be used by them.

This final design report describes shortly the scientific case and in more detail the general layout, the X-ray optics and the attached vacuum system as it was possible in the conceptual design report [1.1]. The results of ray-tracing calculations (with SHADOW), modelling focussing, intensity and resolution will be reported. The description of the experimental end-stations and the scientific equipment will be given in an independent second part of the design report.

2. Scientific Case

2.1. Radiochemical XAS Studies

The Institute of Radiochemistry is interested in research for risk assessment studies and remediation of radionuclide contaminations related to uranium ore mining and processing in the German regions of Saxony and Thuringia and in the neighboring Czech Republic. Closely related to these studies is the research on radionuclide contaminant transport in various regions of Russia and in several successor states of the former Soviet Union. Huge environmental contaminations exist from nuclear weapons production activities and nuclear accidents in the regions of Cheljabinsk in the Ural and Chernobyl in the Ukraine. To date, there is very little knowledge of the radionuclides' chemical state in the contaminated surface soil. Successful and cost efficient decontamination treatments of the soil and remediation strategies depend strongly on this information. During the remediation process, it is necessary to monitor the effectiveness of the chemical treatment methods.

The intrusion of groundwater is considered as one possible accident scenario. Understanding of the dissolution of the solid waste form, the precipitation of secondary solid radioactive phases, and the interaction of soluble radionuclide species with geological and biological material is essential in order to predict the release and migration of radionuclides and their potential damage to the ecosystem.

The studies of the transport and the migration of heavy metals in general and radionuclides in particular in the bio- and geosphere for the above-mentioned research areas are closely related and the scientific information obtained in one specific area can be largely applied to the other areas. The research spans from applied to basic. It is centered around the influence of radioactive materials on the environment and can be classified as radioecology. A basic molecular-level understanding is required to quantitatively describe the mechanisms of radionuclide transport in the environment. This microscopic information is used together with chemical/ mathematical models to obtain macroscopic transport predictions.

Many different methods are necessary to provide the microscopic information that is mandatory for making macroscopic predictions. In addition to conventional techniques such as resonance (NMR, ESR) and optical spectroscopies (IR, UV-VIS), electron microscopy and analytical chemistry, modern highly sensitive methods are needed. They are either laser-based (photo acoustic spectroscopy, thermal lensing spectroscopy, time-resolved fluorescence spectroscopy) or synchrotron-based (X-ray Absorption Spectroscopy, XAS).

XAS is a powerful technique to study many chemical elements in solids, liquids and gases. Due to the high intensity of the synchrotron radiation used, lower concentration levels can be reached than with most conventional methods. This is important for real environmental samples where concentrations may be in the milli- and micro-molar range, or even lower. XAS is an element-specific method and provides information about the oxidation state, the coordination, and the bond length to first, second and even third shell neighbor atoms of a metal absorber. This knowledge is essential to study the interaction of radionuclides such as uranium, thorium, neptunium, plutonium, americium, zirconium, radium, strontium, cesium and technetium with soils, minerals and mineral assemblies. XAS spectroscopy can provide information of the speciation of metals and radionuclides and of speciation changes that result from changes of their chemical environment.

Synchrotron-based X-ray Absorption Near Edge Structure Spectroscopy (XANES) and Extended X-ray Absorption Fine Structure Spectroscopy (EXAFS) will be used at ROBL for the following research areas:

- Speciation and complexation studies of radionuclides in aqueous and non-aqueous solutions pertinent to environmental contamination, pollution risk assessment, and remediation strategies.
- Adsorption processes at the solid-water interface of radionuclide solutions with soils, minerals, mineral assemblies and uranium mill tailings.
- Adsorption and incorporation of radionuclides in biological materials in support of bioinorganic chemistry and bioremediation technologies.

2.2. Materials Science and Structural Studies

The Institute of Ion Beam Physics and Materials Research (IIM) performes investigations concerning the modification of surfaces and the production of thin layers on or below surfaces by ion beam processes. Synchrotron radiation is a powerful tool for the characterization of thin layers and interfaces through the application of gracing incidence techniques.

The modification of solid surfaces by ion beams is governed by different elementary processes (implantation, sputtering, defect formation, relocation of atoms) in dependence on the ion species and ion energy. Ion bombardment of surfaces may influence the surface topography, the surface composition, and the surface structure and thereby the mechanical, electrical and optical properties of the surface. It may also result in thin film deposition or the formation of buried layers.

The IIM in Rossendorf has a broad technical base for the production of ion beams for surface modification, like accelerators and implanters, covering the ion energy range from about 1 keV up to 5 MeV. The research is devoted to the modification of semiconductors as well as metals. These investigations are partly application oriented, partly they concern the basic mechanisms of ion beam modification of materials. Typical current problems include the production of hard coatings on metallic surfaces, the investigation of band-gap engineering by the synthesis of silicides in silicon through ion implantation, or the production of nanocrystalline materials for optical applications in the blue light region by ion techniques. Besides the modification, the ion beams are also used for the analysis of the modified samples. These analysing techniques mainly cover information on atomic composition of films or layers and the depth profile of different elements involved. Concerning surface and interface structure, and also phase composition of the produced layers, there is some gap in the available information which can be filled by surface sensitive X-ray techniques.
Such measurements require X-ray beams of high intensity and small divergence only available from synchrotron radiation sources. Main reasons are the small amount of material within the thin films, the study of weak scatterers (main components of hard coatings) or the recording of diffuse scattering effects, respectively. Moreover, the extension of the photon energy above 25 keV, with an high penetration capability, opens new and unexplored possibilities in the study of buried interfaces.

The aim of the IIM is to characterize layers produced by ion beam techniques and their interfaces as well as to carry out in-situ experiments for the study of phase formation, layer growth and interface development during post-implantation annealing. The different problems will be studied in dependence on surface and deposit material as well as the deposition conditions. In part the same problems are of interest using various other methods of film growth. We will restrict our work to the field of ion beam processes and combine the synchrotron radiation results with other analytical techniques existing in Rossendorf.
The main techniques will be X-ray diffraction and reflectivity (specular and non-specular). There will be foreseen the possibility to use fluorescence EXAFS.

Besides the IIM also groups from universities in Dresden, Chemnitz, and Freiberg are interested in using the materials science part of the beamline. The demands of these groups were taken into consideration when designing the beamline.

Examples of investigations planned at the materials science end-station are:

- Investigations of the phase composition and interface characteristics of buried layers produced by ion implantation. This includes the possibility to study the structural effects of annealing processes, e.g. the Ostwald ripening.
- Investigation of ion induced modifications of interfaces, mainly concerning roughness or thickness. This should give indirect information about the interaction of defects with interfaces or amorphization processes.
- Structural characterization of hard covers. The understanding of the interrelation between atomic structure (amorphous phases, metastable and stable crystalline phases) and physical properties of hard covers is important for finding ways to influence the functionality through the modification of the processes of preparation and surface finishing. Structural studies in statical and dynamical mode (during annealing) are envisaged.
- Analysis of density changes of hard covers produced by an IBAD (ion beam assisted deposition) process during additional ion bombardment.
- Structural investigations of melts and the glassy state. This concerns the determination of the short range order in metallic melts from far above the melting point till down to the undercooled state. Also the crystallization process or the corresponding structure of the glassy state will be studied. The use of anomalous dispersion for the estimation of partial structure functions will be an advantage of such experiments.
- Investigation of ordering and phase formation in metal-metal as well as $A^{III}B^{V}$-semiconductor nanometer-multilayers. The understanding of property-anomalies (mechanical, electrical, magnetic, optical) of the multilayers, the characterization of the structure, short-range order parameters, roughness or diffusion coefficients of the interface region concerned is essential for the defined modification.
- Analysis of the real structure of single crystallites. Study of fundamental and quasi-forbidden reflections with high spatial resolution for defect mapping. Analysis of the reflection profile and the orientation of single crystallites in polycrystals for the understanding of the deformation behaviour of multi-component materials.

The experimental equipment of the materials science end-station will be designed for experiments on thin film systems, liquid surfaces, and special Bragg diffraction techniques on polycrystalline materials.

3. Layout of the Beamline

This chapter describes the distribution of the available floor space in the sector for the beamline BM20 in the experimental hall of the ESRF. Since the handling of radiochemical samples is a new point for the ESRF, a description of the special safety aspects will be given.

The experimental arrangements and the space requirements for the equipment for both types of experiments, radiochemistry and materials science, are quite different. Therefore, two independent experimental endstations in separate hutches were planned. Furthermore, it was decided to run the experiments in both hutches alternatively. There was no case to split the beamline into two branches as realised in the SNBL or DUBBLE CRGs [3.1].

3.1. The Structure of the Beamline

The beamline´s outer structure will be built up from hutches and cabins. Hutches stand for lead shielded structures where the synchrotron radiation beam hits optical elements or the sample. The full lead shielding of the structure prevents the transmission of radiation to freely accessible part of the experimental hall. During experiments with the X-ray beam access to the hutches is forbidden and preventes by a personnel safety system (PSS). Cabins are light weight room structures for housing control and measuring equipment or sample preparation.

The beamline will be aligned towards the high field section of a bending magnet with a critical energy of 20.4 keV (0.85 T magnet section). The high field region of the bending magnet source extends from 6 to 12 mrad, so a maximum horizontal divergence of radiation of 6 mrad can be used. The ROBL will use 2.8 mrad of this fan centered at 9 mrad.
A general picture of the structure of the beamline is given in Fig. 3.1.

The photon beam delivered by this source enters the experimental hall in a distance of 22.54 m from the source point. The optics hutch (OH) will be located immediately behind the shielding wall of the storage ring.

The radiochemistry hutch (RCH) is dedicated to radiochemical XAS experiments. It is the first experimental hutch located directly behind the optics hutch. The sample position is located near the 1:3 demagnification point of the beamline optics. The main element of the experimental setup is a glove box for handling low radioactive samples. The use of radioactive samples implies a specification of the hutch as a radionuclide laboratory of class B with appropriate measures for contamination protection. In particular, to enter the hutch a special lock must be foreseen (RCL). The activity which can be handled in the class-B-laboratory ranges from 370 kBq to 370 MBq (10 µCi to 10 mCi). The upper limit was reduced to 185 MBq because of internal regulations at the ESRF.

The second experimental area is dedicated to materials science experiments. The materials science hutch (MRH) is centered at 54 m from the source point.

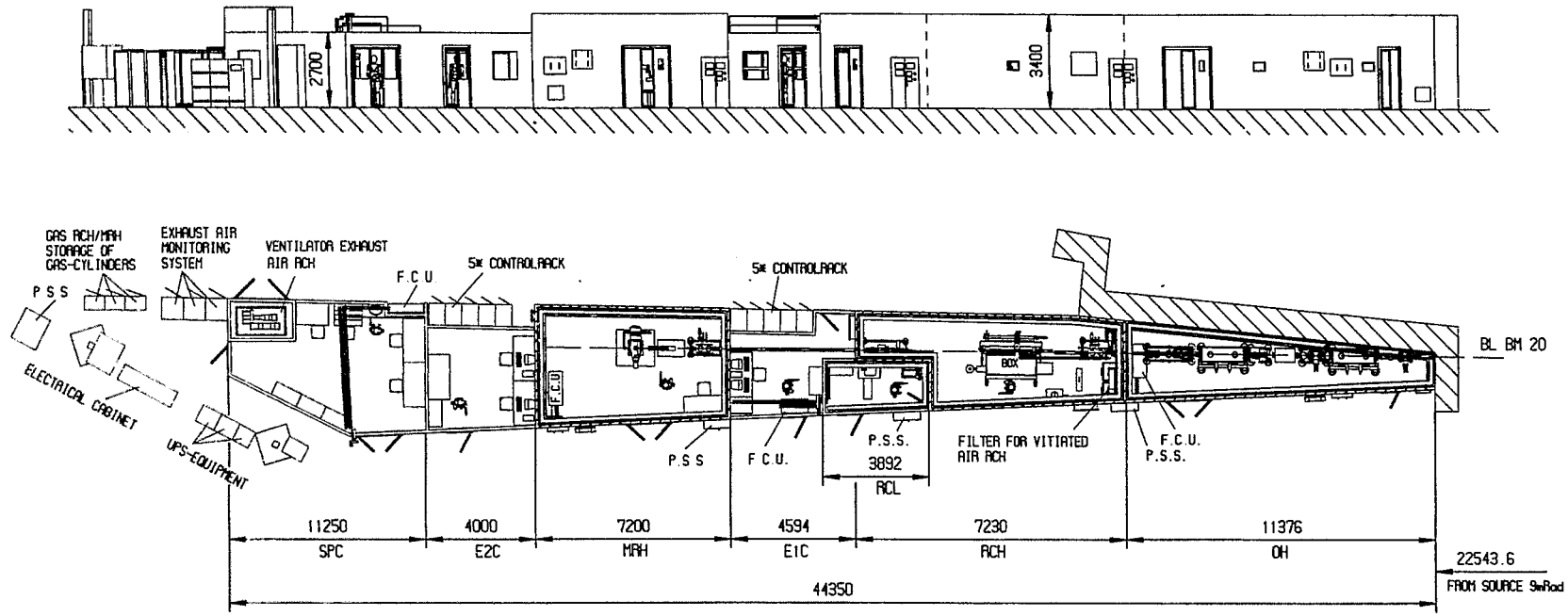

Fig. 3.1: Layout of ROBL at the beam port BM20 of the ESRF.
The lead shielded hutches for optics (OH), radiochemistry experiments (RCH) and materials science experiments (MRH) as well as the cabins for controlling the first and second experiments, respectively (E1C, E2C), and for normal sample preparation are indicated. PSS is the personnel safety system and FCU are fan cooling units for air-conditioning.

This is the region of 1:1 demagnification mode of the beamline optics. The area of this hutch has a dimension of about 4x7 m^2. In the front part a multi-purpose goniometer for X-ray scattering experiments will be installed. The back part is open for additional experimental equipment to be installed in a later stage.

The optics and the experimental hutches are constructed according to the plans approved by the ESRF. The design is based on standard segments of 1 or 2 meters length and additional elements for fitting to the total length of hutches. The roofs have moveable hatches in order to bring in the equipment. At various positions of the hutches sidewalls windows are installed in order to allow visual inspection of the equipment while the synchrotron radiation is "ON" in the hutch. The opening system for the doors is connected to the personnel safety system (PSS), according to the regulations of the ESRF.

The connection of electricity, water, gas, air etc. to the instrumentation within the hutches will be performed through schikanes, in order to guarantee the radiation safety.

The radiation shielding of the hutches consists of 6 mm lead for the optics hutch and of 4 mm lead for the experimental hutches, where only monochromatic beam can enter. Special attention is paid to the radiation tightness in the regions where the hutch walls meet the floor and the concrete wall of the storage ring. There are located additional lead shields.

The smaller part of the floor space of BM20 is occupied by cabins. The control cabins E1C and E2C are located behind each of the experimental hutches. The cabins house the equipment for running the experiments and for data aquisition. The control racks in each cabin are shared between the experiment specific electronics and the general beamline/optics control electronics. The monochromatic synchrotron radiation beam has to pass through E1C in order to reach the MRH. The vacuum tube for the beam will be shielded by a 6 mm lead jacket. At the end of the floor sector there is a sample preparation cabin (SPC). It will be used for sample preparation for the materials science experiments (not for radiochemistry) as well as for off-beam maintenance, repair and adjustment of beamline components.

The air-conditioning of hutches and cabins (except for RCH, see below) will be performed by fan cooling units. The temperature stability should be $\pm$0.5 deg. in the optics hutch, $\pm$1 deg. in the materials science hutch and $\pm$1.5 deg. in the cabins.

3.2. Safety Aspects for the Radiochemical Experiments

Special requirements have to be fulfilled for the radiochemistry hutch. The declaration of the hutch as a radiochemical laboratory of class B means that one can handle open sources of nuclides of the radiotoxicity group I up to a maximum activity of 370 MBq. *Open sources in the legal sense* are not confined in approved and nearly nondestructable containers (e.g. from stainless steel). The condition is that such containers can only be opened with special instruments. In the experiments the samples will generally be enclosed in containers normally made of polyethylen. In the common sense these sources will not be open.

There is no sample preparation at the ESRF site for the radiochemistry experiments. All samples will be prepared in Rossendorf and shipped in approved containers to Grenoble. An intermediate storage of samples at the Institute Laue-Langevin (ILL) is foreseen and the regulations for access to the ILL storage are fixed in a contract between ESRF and ILL. The amount of activity present at ROBL is normally limited to 74 MBq and only by special permission of the ESRF to 185 MBq.

All procedures for the sample handling and the general design principles for the radiochemistry hutch and the experimental equipment were agreed between the FZR and the ESRF. They are part of the „Declaration to the Prefecture of Grenoble". The radiochemical work at ROBL was according to the French law permitted by the prefecture of Grenoble on October 3, 1995.

To guarantee a safe operation of the radiochemistry experiments and to monitor the actual status, the following design features will be realised:

- The sample transport is always performed in certified containers.
- The activity of the samples can be controlled inside the glove box.
- The sample positioning into the beam will be made in the glove box.
- A three barrier concept will be realised.
- The inner wall of the RCH is made as a "chemical confinement" for high tightness and easy decontamination.
- The RCH will have a special ventilation with filtering and monitoring of the exhaust air. All critical parts are installed redundant.
- The RCH can be reached only by passing a lock room with personal monitoring equipment. The access to and operation of the radiochemistry experiments is limited to authorized personnel.

For the layout of the beamline structure the last four points are of importance.

The barrier concept is illustrated in Fig. 3.2. The samples are always enclosed in a container serving as the first barrier. The sample container itself is either inside a multi-walled transport container or within the glove box. The glove box is the second barrier under normal experiment conditions. The glove box is located in the hutch which is a third barrier in regard to the experimental hall of the ESRF. The negative pressure gradient hall-->hutch--> box will be established by the special ventilation system for the RCH.

The air conditioning/ventilation system of the RCH is separat from the other systems. It will perform 8 complete changes of air per hour. There are separate ventilators for the glove box exhaust air and the general hutch exhaust air, each with filters for aerosols. The separate ventilators allow for a pressure difference between glove box and hutch. The exhaust air will be controlled by a monitoring system outside the RCH to prevent background effects. At the end the filtered and monitored exhaust air will be transported outside the experimental hall and released over the roof of the hall.

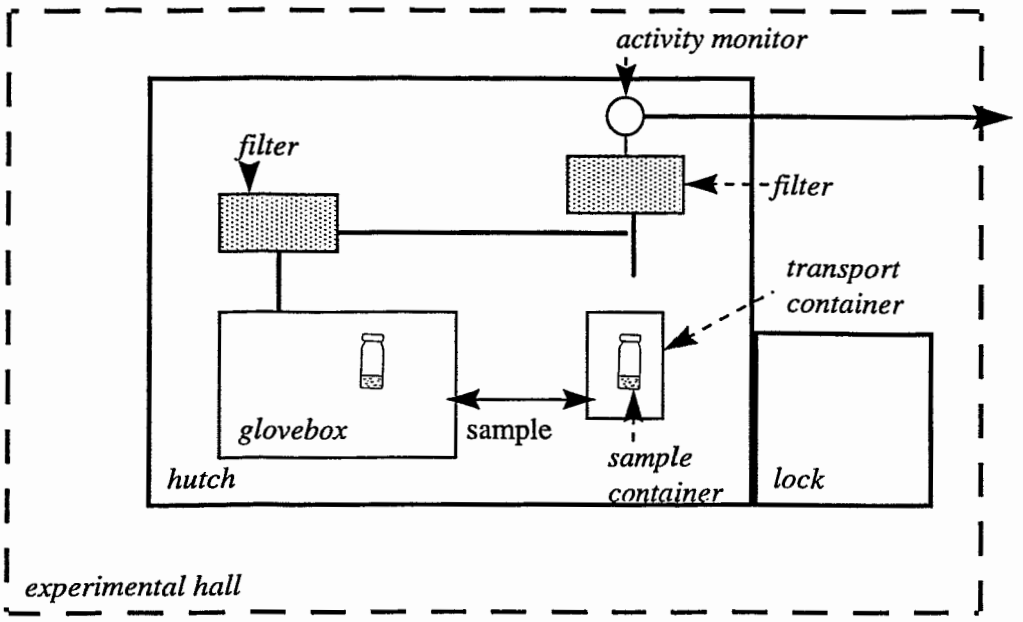

Fig. 3.2: Barrier concept of the radiochemistry hutch of ROBL.

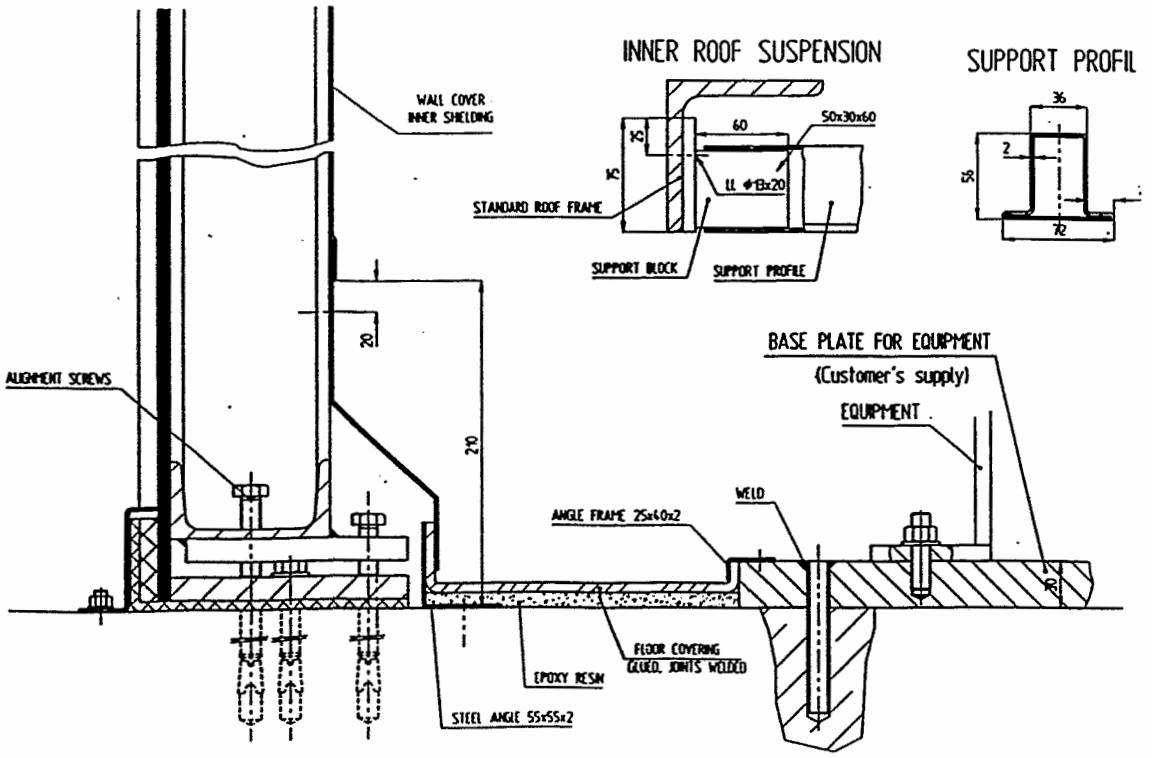

Fig. 3.3: Cross section through the wall and floor of the radiochemistry hutch. The additional "chemical confinement" is realised by steel panels at the wall and plastic covering of the floor. All equipment will be mounted on plates in order to prevent the original floor of the experimental hall from any possible contamination.

A "chemical confinement" will be installed at the inner wall of the radiochemistry hutch. The two functions to be achieve are: (i) a good air tightness of the hutch (to allow for a pressure gradient to the hall) and (ii) to provide a plane surface (for the case that decontamination measures will be necessary). Fig. 3.3 shows a cross section through the wall and floor area of RCH. The wall confinement consists of steel panels screwed to the standard wall structure. The connections between the panels are tightened by resin parts and the panels are painted with special decontamination paint. On the floor there is a highly resistent plastic floor covering. The equipment is mounted on plates. The interface between the floor covering and the walls as well as the mounting plates will be tightened by epoxy resin.

The access to RCH is possible only through the lock room (RCL in Fig. 3.1). There a change of coats and shoes has to be performed. After leaving the RCH the experimenters have to check themself with the personnel monitor for contamination.

4. X-Ray Optics

The function of beamline optics is to deliver a synchrotron radiation beam of the desired characteristics to the experimental end-stations. The demands of the two typical experimental arrangements for radiochemistry and materials science, respectively, are quite different. The design goal was to find an optimal physical solution which is technically realistic.
This chapter describes the design principles and the final specifications for the layout of the X-ray optics.

4.1. Demands for the Optics

The demands for the design of the beamline optics were the following:

- energy range: 5 keV .... 35 keV
- energy resolution: $\Delta E/E \leq 10^{-4}$
- standard beam: vertically parallel / horizontally slightly focussed
- maximum focussing: $\leq 0.5 \times 0.5$ mm^2 at the radiochemistry experiment
- suppression factor for higher harmonics: $<10^{-3}$
- possibility for QEXAFS: scan of 1 keV in 100 seconds

The energy range was determined by the demand to have access to the maximum possible number of elements for XAS investigations. Fig. 4.1 shows the energy of the absorption edges versus the atomic number [4.1]. The maximum energy of 35 keV which should be transmitted by the optics allows the investigation of all heavier elements by switching from the K-edge to the L_{III}-edge. The limitation to 35 kev is caused by the use of X-ray mirrors. The minimum energy of 5 keV is determined by the absorption from the beryllium windows which are in the beam for safety reasons (cf. 4.6.5.).

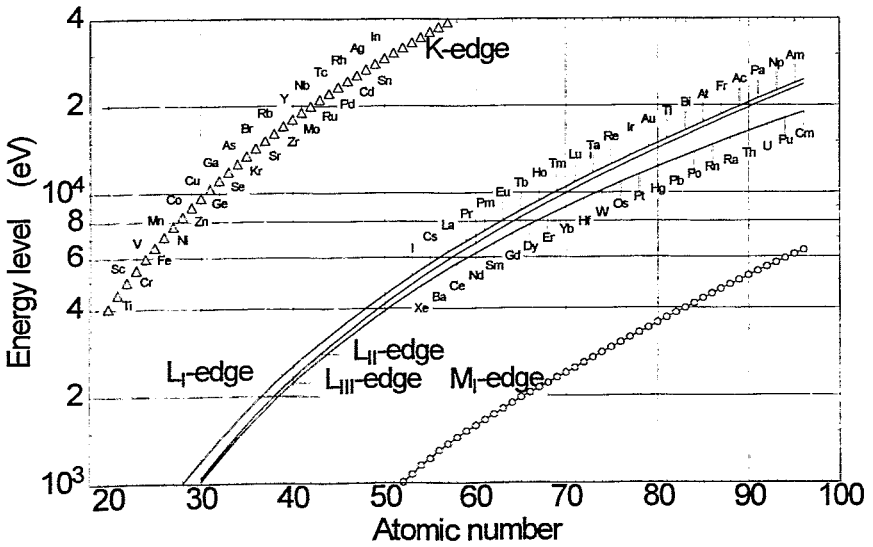

Fig. 4.1: Energy of the different absorption edges of the elements versus atomic number.

The demand of an energy resolution better than 10^{-4} results from XANES experiments to be performed. In order to study the structure of the absorption edge the energy resolution should be better than the edge width. The relative energy widths of the K-egdes are typically $>2x10^{-2}$ and the widths of the L_{III}-edges $>4x10^{-4}$.
In the standard experiments one will have a vertically parallel beam of about 3 mm height and horizontally a slightly focussed beam which is about 20 mm in width at the materials science end-station.

For the radiochemistry experiments there is a certain interest to make "point-by-point investigations" of (e.g. geological) samples in order to map element distributions. From this results the demand for maximum focussing of the beam. Bearing in mind the characteristic parameters of the bending magnet source, a focussing down to 0.5x0.5 mm^2 (FWHM values) seems realistic.

Since the synchrotron radiation spectrum is continuous, a beam monochromator can also pass energies of $n \cdot E_0$, where E_0 is the selected energy for the experiment. These so called harmonics should be suppressed otherwise one can have significant problems in the data evaluation, in particular in XAS-experiments.

For the study of the kinetics of different processes a Quick-EXAFS experiment should be possible. For the specification of the optics the scanning of 1 keV within 100 seconds was taken as the design parameter.

4.2. Structure of the Beamline Optics

According to the demands given in the previous section the main optical problems to be solved in the beamline concept are the variable focus and the harmonic rejection. In analogy to existing beamlines at ESRF a system mirror - double crystal monochromator - mirror will be used. These are the main optical elements which determine energy, resolution and focussing. Besides them there are additional optical components for beam size control and intensity definition as well as beam diagnostics.

The top and the side views of the structure of the beamline optics are given in Fig. 4.2. Only the main components (monochromator and mirrors) are shown.

The vertical collimation/focussing should be accomplished by the mirrors while sagittal focussing is achieved by the second crystal of the double crystal monochromator. Indeed, the physical separation of the horizontal and vertical focussing has many advantages from an optical point of view, both in terms of alignment and stability (since horizontal movements of source or optics do not couple directly to vertical movements).

The first mirror will be used for vertical focussing at infinity, since otherwise the vertical divergences of the X-ray beam are too large to obtain the required energy

resolution with perfect crystals as monochromator. The second mirror either reflects the parallel beam to the experiment or makes the final vertical focussing. A further advantage of using a pair of mirrors in front of and behind the monochromator is the fact that the beam direction can be conserved. In dependence on the material for the reflecting surface of the mirror the energy band pass has a certain upper limit. This limit is essential for the harmonic rejection.

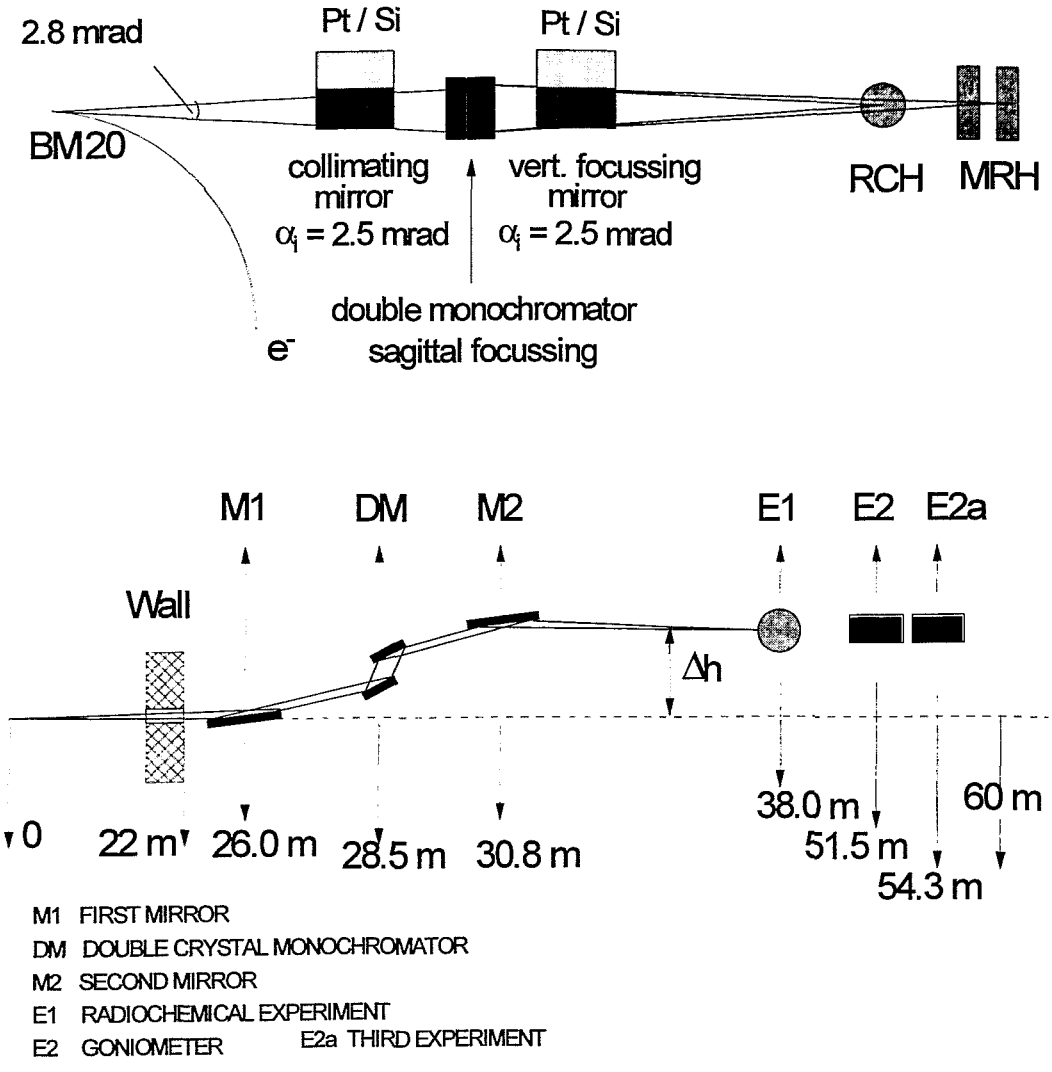

Fig. 4.2: Top view and side view of the beamline optics scheme of ROBL.

The double crystal monochromator consists of two identical perfect crystals which will be tuned to select by Bragg scattering a certain energy out of the continuous spectrum of the source. The perfection of the crystals determines the energy resolution to a large extent. A fixed exit geometry of the monochromator will be realized. The accuracy of the setting of the first crystal determines the accuracy of the selected X-ray energy (wave length). The second crystal should be saggitally bent in order to achieve horizontal focussing of the beam.

In the following sections the optical elements will be described in more detail.

4.3. Source Characteristics

The charcteristics of the storage ring and the bending magnet source of the ESRF [4.2] are given in Table 4.1

Table 4.1: ESRF machine characteristics [4.2, 4.3]

electron beam energy	E = 6 GeV
current in the multibunch mode	I $\geq$ 200 mA
horizontal emittance	$\varepsilon_X = 4 \times 10^{-9}$ m *rad
vertical emittance	$\varepsilon_Z \leq 8 \times 10^{-11}$ m *rad
beam lifetime	$\tau \geq 12$ h
magnetic field of bending magnet	B = 0.85 T (Radius=23.4m)
critical energy of bending magnet	E_C = 20.4 keV

Energetic electrons emit a highly collimated and intense flux of high energy photons, while a high brilliance is obtained due to a low emittance.
The flux of synchrotron radiation emitted from bending magnet of ESRF is shown in Fig. 4.3 as function of energy.

The charcteristics of the electron and photon beams at the bending magnet source at the ESRF [4.2] are listed in Table 4.2

Table 4.2: Source electron and photon beam parameters at the ESRF bending magnet σ and are r.m.s. values of source size (x, z) and divergence (x',z'); $\Delta\Phi$ is the angular fan of the photon beam

electron beam				photon beam	
σ_X [μm]	σ_Z [μm]	$\sigma_{X'}$ [μrad]	$\sigma_{Z'}$ [μrad]	$\Delta\Phi$ [mrad]	σ_r at crit.energy [μrad]
187	128	115	5	6	49

The electron beam in the bending magnet has a very low vertical divergence, ten times lower than the radiation's natural divergence at the critical energy, and about seven times smaller than the lowest value of σ_r (at 50 keV). Therefore one can neglect the convolution between the vertical divergence distributions of the emitted photons (σ_r) and the electron beam ($\sigma_{Z'}$).

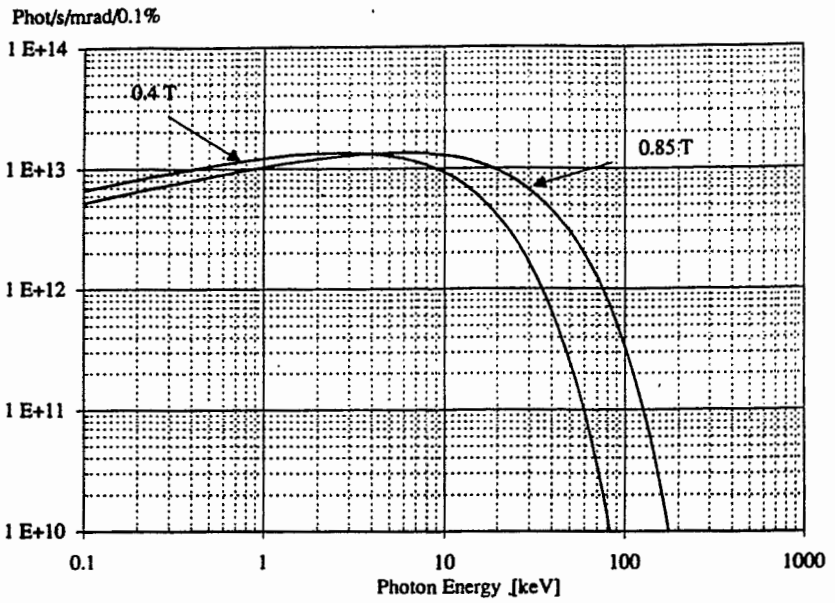

Fig. 4.3: Vertically integrated photon flux from the bending magnet source of the ESRF. ROBL will use the high field section with B = 0.85 T.

In order to calculate the values of power density on the mirrors and diffracting crystals in the monochromator we consider the power emitted by the bending magnet, which is a function of the angle of elevation from the horizontal [4.4]:

$$P[\,W / mrad\ \phi\ mrad\ \psi] = 1285.6\ F(\gamma\psi) \qquad (4.1)$$

with

$$F(\gamma\psi) = \{7/16 + 5/16\ (\gamma\psi)^2 / [\,1 + (\gamma\psi)^2\,]\}\,[1 + (\gamma\psi)^2\,]^{-5/2} \qquad (4.2)$$

and $\gamma = E/m_0c^2$, ϕ is the horizontal opening angle and ψ is the angle of elevation from the orbit plane.
For an unlimited vertical acceptance we get for the ESRF bending magnet the vertically integrated power density

$$P' = 156\ Watts/\ mrad\ \phi \qquad (4.3)$$

In the ROBL design a 2.8 mrad horizontal fan of radiation is collected at the bending magnet port. Therefore, the total power entering the beamline is:

$$P = 436\ Watts \qquad (4.4)$$

4.4. X-Ray Mirrors

4.4.1. Functions and Principle of the Mirrors

The X-ray mirrors have two functions which are based on different physical principles:

- suppression of the high energy part of the radiation spectrum
- collimation or focussing of the beam

While the second point can be achieved simply by bending a flat mirror or giving the mirrors surface an appropriate shape, the solution for the first point depends on different aspects.

The X-ray mirror makes use of the total reflection of radiation. In the total reflection regime the absorption of X-rays can be ignored and from the complex refractive index n

$$n = 1 - \delta + i\beta \tag{4.5}$$

one has to deal with the real part δ only [O5]. The critical angle θ_c below which total reflection occurs is related to δ by:

$$\theta_c \approx \sqrt{2\delta} \tag{4.6}$$

More explicitely one obtains

$$\theta_c \approx 2.324\sqrt{Z\rho / A} * \lambda = 28.808\sqrt{Z\rho / A} / E \tag{4.7}$$

The critical angle θ_c is given in mrad if the X-ray wavelength λ is given in Å or the X-ray energy E in keV. Z is the atomic number, ρ the mass density and A the atomic weight of the reflecting material.

For the choice of the reflecting material of the mirrors there are three points which have to be respected:

- The energy cut-off in reflectivity at a given incidence angle θ_i.
- The available heigth of the mirror perpendicular to the beam is limited by the technically available mirror length for a given angle of incidence. This height determines the percentage of the primary intensity accepted by the mirror.
- The position of absorption edges of the reflection material. Although the mirror works in the total reflection regime, there are distortions in the reflected intensity near absorption edges.

Table 4.3 gives an overview about the different parameters for typical mirror materials used for synchrotron radiation application. Besides the critical angles calculated for different X-ray energies the positions of the absorption edges are given. The latter are important for estimating the pertubations in the reflected X-ray spectrum.

Since one of the demands to the X-ray optics was the use of energies up to 35 keV one has to select Rh, Pd, Pt or Au for the mirror material. Otherwise the critical angle becomes to low. Pertubations in the reflected spectrum are generally less for rhodium. There is only one absorption edge at 23 keV compared to the 3 L-edges of Pt and Au. On the other hand, the L-edges of the actinides are located around 20 keV and as the study of actinides is one main goal for this beamline, platinum therefore is the better choice for the mirror material.

Table 4.3: Collection of data for typical materials for synchrotron radiation mirrors. The critical angle, θ_c are calculated for different X-ray energies. The absorption edges are given for an estimate of perturbations in the reflected beam.

Material	Si	Ni	Rh	Pd	Pt	Au
Z	14	28	45	46	78	79
ρ (g/cm^3)	2.33	8.88	12.41	12.0	21.45	18.9
A	28.09	58.69	102.9	106.4	195.09	196.97
θ_c (mrad) @ 35 keV	0.887	1.707	1.934	1.89	2.341	2.286
θ_c (mrad) @ 30 keV	1.035	1.977	2.238	2.19	2.813	2.645
θ_c (mrad) @ 25 keV	1.242	2.371	2.685	2.625	3.376	3.17
θ_c (mrad) @ 12 keV	2.587	4.941	5.593	5.468	7.03	6.61
K-edge (keV)	1.84	8.337	23.21	24.35	78.35	80.67
L_I-edge (keV)	0.15	1.02	3.404	3.614	13.865	14.351
L_{III}-edge (keV)	0.099	0.858	2.995	3.181	11.55	11.92

The second aspect is the percentage of primary radiation which will be accepted by the mirror of a given length. This is determined by the divergence of the beam from the source as well as by the combination of mirror length and angle of incidence. The beam divergence at a low emittance synchrotron radiation source is fully described by the divergence of the production of synchrotron radiation by the single photon process. In the energy range of interest for ROBL the divergence can be described by a Gaussian. The FWHM can be calculated from the approximation for the r.m.s. divergence σ given in [4.6].

$$FWHM = 2\sqrt{2\ln 2}\sigma = 2.355\frac{0.565}{\gamma}(E_c / E)^{0.425} \qquad (4.8)$$

with γ = 11742. The FWHM is given in µrad and E_c is the critical energy of the source, i.e. 20.4 keV for ROBL.

In dependence on the energy of the synchrotron radiation the vertical divergence can be calculated. The first mirror of ROBL will be located at 26 m from the source point and for this distance the vertical beam height at FWHM z_{FWHM} was estimated. Finally, the percentage of radiation accepted by a mirror (P_{acc}) at this distance of 26 m with a visible height vh was calculated from the area under a Gaussian of FWHM integrated from -vh/2 to +vh/2.
The values of FWHM, z_{FWHM} and P_{acc} are given in Tab. 4.4 versus the energy of the synchrotron radiation. As typical visible heights vh of the mirror the values 3 mm, 2.5 mm, and 2 mm were chosen. From the technical point of view X-ray mirrors as long as 1 m or 1.2 m are possible. The interrelation between visible height vh and the angle of incidence α is given in Table 4.5.

By the choice of 3 mm intercepted beam height the mirror collects always about 10% more of the primary intensity compared to 2.5 mm intercepted height. As can be seen from Table 4.3 the demand of a maximum energy of 35 keV can be realized with common coating materials only with angles of incidence below 2.5 mrad. Though a maximum of accepted primary intensity can be reached with

mirrors longer than 1.2 m. Such mirrors are technically not standard and quite expensive.

Table 4.4: Divergence of the primary beam FWHM, fan size at FWHM in a distance of 26 m from the source and percentage of accepted primary intensity P_{acc} for mirrors of different visible height vh in dependence on energy.

Energy (keV)	5	10	15	20	25	30	35
FWHM (µrad)	206	153.4	129.1	114.3	103.9	96.2	90
fan size at FWHM at a distance of 26 m from source	5.36	3.99	3.36	2.97	2.70	2.50	2.34
P_{acc} @ vh = 3 mm (%)	<50	62.2	70.6	76.3	80.8	84.0	87.1
P_{acc} @ vh = 2.5 mm (%)	--	53.7	61.8	67.7	72.2	75.9	79.0
P_{acc} @ vh = 2 mm (%)				57.7	61.6	65.1	68.9

Table 4.5: Angle of incidence α for a X-ray mirror of different length l and a given visible height vh.

α (mrad) ↘	vh = 3 mm	vh = 2.5 mm	vh = 2 mm
l = 1200 mm	2.5	2.08	1.67
l = 1000 mm	3.0	2.5	2.0

Therefore, the optimum choice for the mirror allowing to use energies up to 35 keV at the beamline is a 1.2 m long mirror coated with platinum. It accepts about 75% of the source intensity at the critical energy of 20.4 keV.

The choice of substrate material for the mirror is influenced by several properties (mechanical stability, thermal conductivity, thermal expansion coefficient, density, Young's modulus, Poisson's ratio and, polishing capability) which are important for the quality of the mirror. The crucial point is the managing of the heat load on the mirror. The first mirror will be water-cooled and made from single-crystalline silicon. For the second mirror in the monoenergetic beam behind the monochromator no heat load problem occurs and the substrate material can be ZERODUR.

4.4.2. Harmonics Rejection

In the case of XAS-experiments harmonics passing through the monochromator can influence the results significantly. This effect mainly depends on the composition of the sample under investigation.
Fig.4.1 shows the absorption edges of the elements and can illustrate the effect of higher order radiation. If for example, the Fe-edge at 7 keV should be measured and the sample contains also uranium or neptunium, then a 3rd order harmonics at 21 keV can give absorption at the heavy nuclei. Since also the basic energy of absorption in the Fe-case is attenuated by Eu-L_{III} the effect that certain element combinations are excluded from investigation is not only a

problem of harmonics. However, due to harmonics the number of elements excluded from simultaneous investigation is increased.
The problem arises mainly when using lower energy synchrotron radiation (5-15 keV) for the experiments. At higher energies the intensity from the source drops down quite rapidly and thereby the effect of harmonics also.

However for a certain choice of the reflecting crystal plane in the monochromator some harmonics do not occur. For ROBL it is proposed to use single crystals of silicon with the reflecting planes (311) and (111) as monochromator. For this choice only the threefold of the selected energy has to be suppressed. The intensity of higher order harmonics contributing to the experimental spectrum depends on the incident spectrum of the synchrotron radiation source as well as the transmission band path of the mirror system used in the optics.

The main effect for the harmonics rejection has to be achieved by the X-ray mirrors. It is noted, that a small mis-setting of the second perfect crystal of the double crystal monochromator partly can also be used for harmonics rejection. This method will not be discussed in detail because it may not be applicable if the second crystal of the monochromator is bent for sagittal focussing.
Commonly, the suppression of harmonics by a factor of 10^{-3} is demanded. With respect to the overall energy range of usable radiation at ROBL for the energies between 5 keV and 12 keV harmonics rejection is then required.
There are two possibilities for the mirror layout to combine wide band path (5-35 keV) with harmonic rejection for the lower energy range (5-12 keV):

- use of one mirror set and two different angles of incidence of the radiation
- use of two sets of mirror materials and the same angle of incidence of the radiation

The first case is illustrated by Fig. 4.4. The reflectivity of two platinum mirrors in dependence on the energy of the radiation is shown. The nominal setting of the mirror, as discussed in the previous paragraph, is an angle of incidence of α = 2.5 mrad. The lowest usable energy is 5 keV, so that 15 keV as third order has to be suppressed appropriately. The required harmonics rejection of 10^{-3} can approximatly be achieved with an incidence angle α = 7.5 mrad.

The two operation modi of the beamline require a setting of the mirrors to α = 2.5 mrad for working in the high energy region and to α = 7.5 mrad for the energies below 12 keV. The consequence of using different incidence angles is that the beam has different heights at the experiment's positions in dependence on the operation mode. The height difference depends on the distance of the two mirrors. For a expected mirror distance of 5 m the beam will be shifted upwards at the experiment's position by about 50 mm by changing from 2.5 mrad to 7.5 mrad.

The second design version is to use mirrors of different coating materials. Light material has a low reflectivity for high energies due to a low critical angle θ_c as seen from Table 4.3. A good candidate is silicon. It is a stable material and can

be polished to low roughness. Moreover it is often used as substrate material. The operation modi in this second design version require mirrors with different surface coatings for using the high energy regime (platinum mirrors) or the low energy regime (silicon mirrors). In both cases the angle of incidence is fixed.

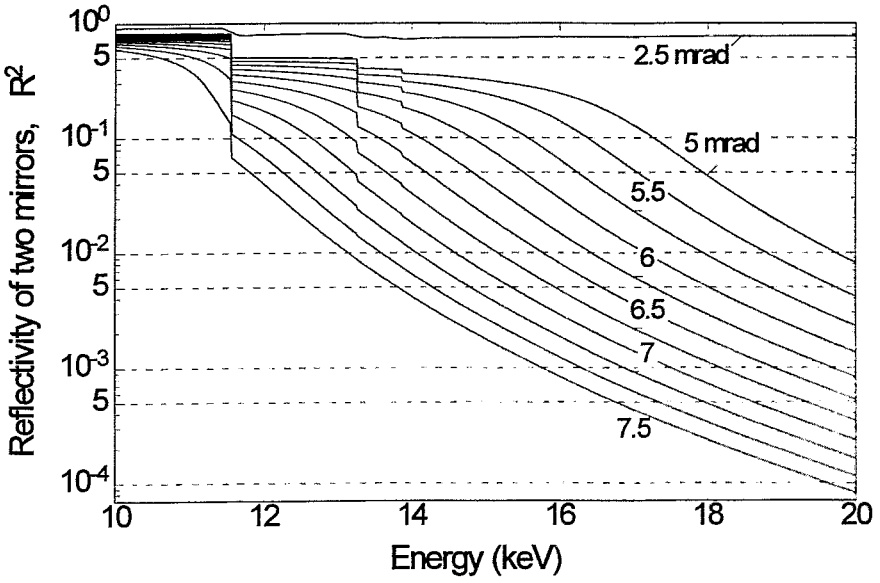

Fig. 4.4: Calculated reflectivity of two platinum mirrors versus energy of radiation for different angles of incidence α.

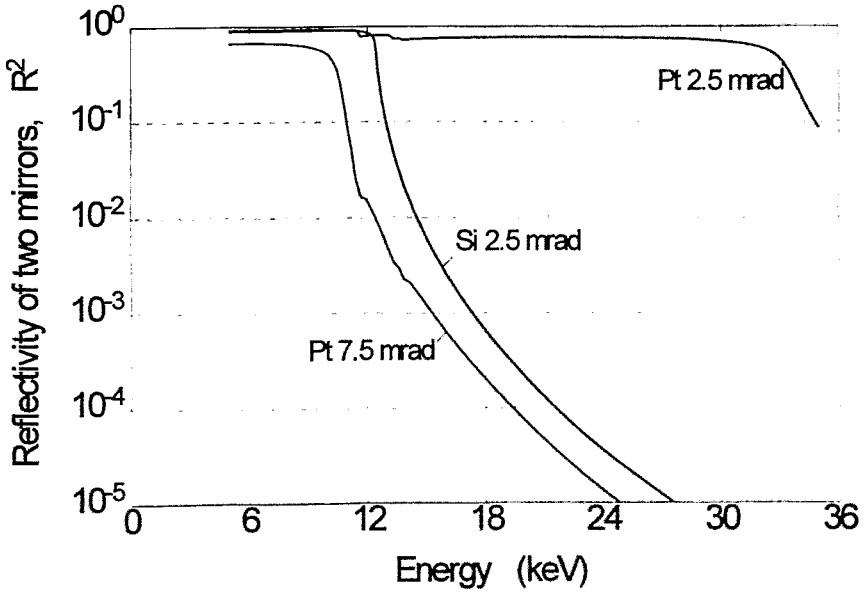

Fig. 4.5: Calculated reflectivity of two mirrors coated with platinum or silicon. A pair of silicon mirrors with an angle of incidence of α = 2.5 mrad has nearly the same reflectivity as a pair of platinum mirrors set to α = 7.5 mrad.

In Fig. 4.5 the reflectivities of a pair of mirrors are compared for platinum coated mirrors with angles of incidence of α = 2.5 mrad and α = 7.5 mrad with silicon coated mirrors with an angle of incidence of α = 2.5 mrad. It can be seen that the reflectivity of silicon mirrors with α = 2.5 mrad has a similar energy dependence as the platinum mirrors with α = 7.5 mrad. A reflectivity drop to 10^{-3} is reached only for E = 17 keV for the silicon mirrors instead of about 15 keV for the platinum mirrors. This causes some limitations for harmonic rejection for nominal energies up to 5.7 keV.

4.4.3. Mirror Design

Comparing the different possibilities as discussed above and taking into account general aspects the following specifications were made for the mirrors of ROBL:

- mirror dimension: 1200 mm x 150 mm
- mirror coating: platinum / silicon (two strips on the same substrate)
- angle of incidence: 2.5 mrad (fixed)
- substrate / cooling: first mirror: silicon single crystal / water cooled
  second mirror: ZERODUR / uncooled
- min. radius of curvature: 5.3 km (second mirror)
- micro-roughness of surface: < 0.5 nm r.m.s.
- slope error: < 1" r.m.s. (meridional) / < 5" r.m.s. (sagittal)

The principle set-up for the first mirror is shown in Fig. 4.6. The two strips of different coating are side by side. The first, cylindrically curved, mirror collimates the incident radiation producing a vertically parallel beam on the first monochromator crystal. For changing from high to low energy mode of the beamline, the mirrors have to be shifted perpendicular to the beam. All other settings are conserved.

The use of two different materials for the mirror coating has the advantage of a constant beam height at the experiments independent on the operation mode (high or low energy). This is very important since there are strong restrictions concerning the air tightness of the radiochemistry hutch. A change of the angle of incidence at the mirror and consequently of the beam height at the experiment by about 50 mm would demand a height change in all equipment behind the first mirror. This concerns in particular the vacuum tubes for the synchrotron radiation beam going in and out of the radiochemistry hutch. The problem of tightness for maintaining the pressure gradient (c.f. 3.2.) would become very crucial in this case.

Another disadvantage of using two different angles of incidence on the mirror would be the necessity to readjust the whole beamline when switching from the high to the low energy mode of operation. However, it can be expected that in the course of the radiochemical studies not only the actinide elements of a sample are of interest but also lighter elements (e.g. transition metals) of the same sample. In such case a quick change from high to low energy mode is necessary.

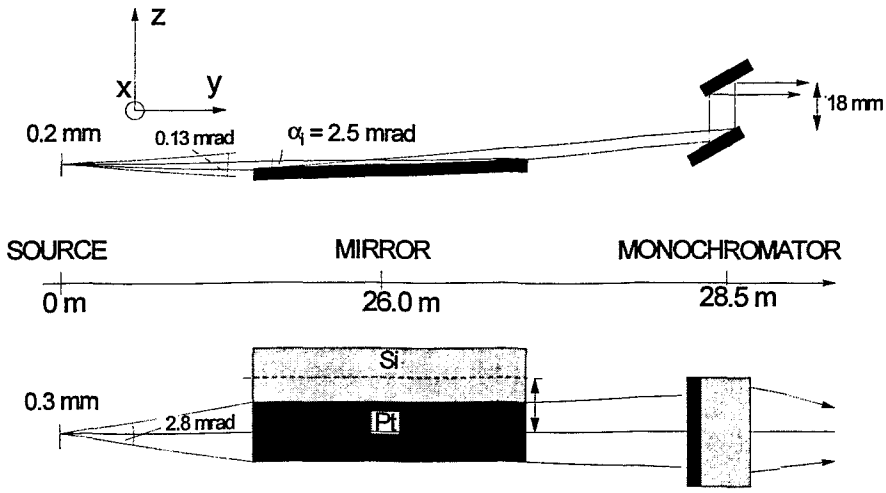

Fig. 4.6: Scheme of the mirror design for the first mirror of ROBL. The two different reflecting coatings of silicon and platinum are brought side by side onto the same substrate. The mirror is always kept with the same angle of incidence of radiation of 2.5 mrad. The source sizes and divergences are also indicated.

The use of two mirror materials is more advantageous, since only the position of the reflecting strip of the mirror has to be changed by overall translation of the mirror. Adjustment procedures are reduced to fine tuning the mirror to optimal intensity. The advantages of the two strip mirror solution has to be paid by some loss in harmonic rejection ability for energies below 6 keV and additional technical efforts for the mirror translation mechanism.

Other specifications like radius of bending, slope error, or micro-roughness influence the performance of the mirror. Their effect was studied also by [4.7, 4.8] and will not be discussed in detail here. The specifications for the ROBL mirrors are within limits which are technically feasible.

4.5. Monochromator

4.5.1. Principle of the Monochromator

In the proposed optical configuration for the ROBL beamline, the monochromator has a dual function:

- selecting the appropriate energy and energy bandpass from the incident white synchrotron radiation beam, and also
- performing a horizontal focussing.

The double crystal monochromator will consist of two separate perfect silicon crystals. Highly perfect silicon single crystals are readily available, have a good thermal conductivity and are also flexible enough for curved crystal optics. The monochromator will be of the fixed-exit type, i.e. the outgoing beam will be fixed whatever the selected energy of X-rays is choosen. The first crystal will be a flat

one and water cooled to avoid distortions due to the thermal load. The second crystal may be bent sagittally for horizontal focussing of the beam.

The choice of reflecting crystal plane depends upon the required resolution. The reflectivity of perfect crystals within the Darwin-width is close to 100%, but the bandpass (and hence transmitted flux) will be reduced for higher indexed reflections. It is proposed to use the odd orders of reflections Si(111) or Si(311), since the even numbered harmonics are forbidden. For experiments which need high flux, e.g. in the fast data collection mode, the more reflective Si(111) plane will be used. The Si(311) cut crystals will be installed for studies where high resolution is required.

The monochromator will have two parallel crystals with fixed entrance. The incident beam will come nearly horizontal with a positive angle of $2\alpha \approx 0.28 \pm 0.06$ degrees, where α is the grazing angle onto the mirror. The beam path in the monochromator is indicated in Fig. 4.7.

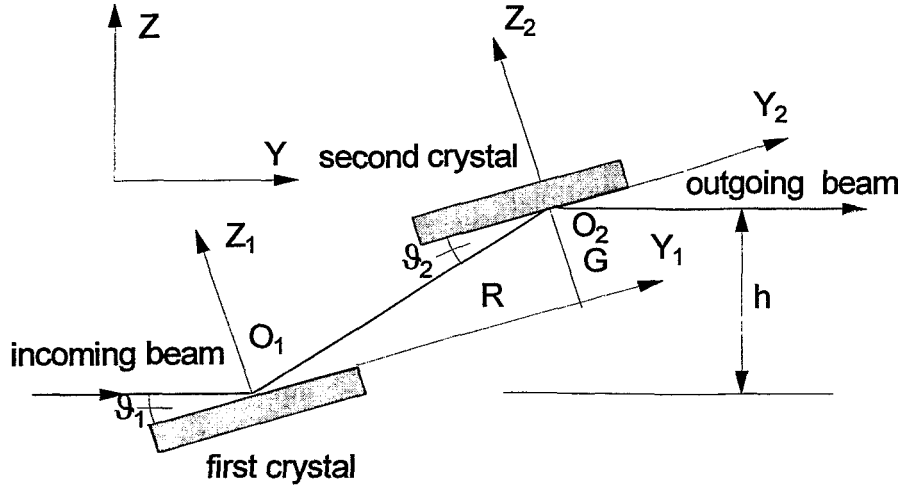

Fig. 4.7: Schematic beam pass in the double crystal monochromator.

The outgoing beam will be higher than the incoming one by h = 18 mm. The center of the fan of the incoming beam defines the vertical reference plane (Y,Z). The design includes only one rotation, called Bragg rotation. The mechanical principle thus results in one rotation, centered on the surface of the first crystal, the rotating plateau bearing two independent translational motions. These move the second crystal in order to keep the output height constant whatever the transmitted energy, and in order to position the beam at the center of this crystal. In the design of the double crystal monochromator the translations are parallel (R) and normal (G) to the diffracting surface.

The translational rail R and the G translation, corresponding to the fixed gap between the two crystals (h), are respectively given by

$$R = h / (2\sin\theta) \qquad \text{and} \qquad G = h / (2\cos\theta) \tag{4.9}$$

The translational components R and G of the vector O_1O_2 between the centers of the diffracting surfaces of the two crystals (these projections are given in the rotating frame along the axes O_1Y_1 and O_1Z_1 of the first crystal in Fig.4.7) and the Bragg angle θ_B for representative energy values in the region of interest (between 5 and 35 keV) are given in Table 4.6 for Si(111) and Si(311). These values R and G define the positions and ranges for the translational stages which move the second crystal unit.

Furthermore, the running in "pseudo channel-cut" mode should be possible, i.e. the only motion in that case is the Bragg rotation (see 4.5.3.). In this mode the desired high data aquisition rate must be paid by a shift Δh of the beam exit height h.

Table 4.6: Bragg angle θ_B, translations R (parallel) and G (perpendicular to the diffraction plane), Δh (shift of the beam in the „pseudo channel-cut" mode for QEXAFS, h = 18 mm) for different values of energy E, and the translation ranges ΔR, ΔG for an energy scan between E and E+1keV

Si (111) **d = 3.1355 Å** **h = 18 mm**

E (keV)	5	6	10	11	20	21	30	31	35
θ_B (deg)	23.30	19.21	11.40	10.36	5.67	5.40	3.78	3.66	3.23
R (mm)	22.75	27.35	45.53	50.05	91.09	95.63	136.52	140.99	159.73
ΔR (mm)		4.6		4.52		4.54		4.47	
G (mm)	9.80	9.53	9.18	9.15	9.04	9.04	9.02	9.02	9.01
ΔG (mm)		0.27		0.03		0.00		0.00	
Δh (mm)				0.06		0.01		0.002	

Si (311) **d = 1.6375 Å** **h = 18 mm**

E (keV)	5	6	10	11	20	21	30	31	35
θ_B (deg)	49.22	39.05	22.25	20.13	10.91	10.39	7.25	7.02	6.20
R (mm)	11.89	14.28	23.77	26.15	47.55	49.90	71.32	73.64	83.33
ΔR (mm)		2.40		2.38		2.35		2.32	
G (mm)	13.77	11.59	9.72	9.59	9.17	9.15	9.07	9.07	9.05
ΔG (mm)		2.18		0.13		0.02		0.00	
Δh (mm)				0.26		0.03		0.01	

The monochromator will be used for two types of experiments: diffraction (experiment at fixed energy) and absorption. The absorption experiments require the more stringent conditions to the double crystal monochromator. In this case, an *energy scan* (i.e. a θ-scan, since $E*\sin\theta$ = const. for a given orientation and a given diffracting crystal) is performed within a typical range of ΔE = 1 keV. One scan includes up to 500 encoded intervals for each of which the data acquisition is done. The smallest interval size should be 10^{-4} degrees. Another point is that,

since in the step-by-step mode the smallest data acquisition time is ≈ 1 second, the dead time should not exceed a fraction of a second (0.1 seconds desired) at each step. Table 4.6 gives the translations R and G for energies corresponding to various absorption scans within the chosen range $5 < E < 35$ keV and the resulting ranges ΔR and ΔG (calculated for absorption scans given by an energy difference $\Delta E = E_1 - E_0 = 1$ keV).

From the Table 4.6 it can be seen that the value R changes almost continuously over the energy range, while for the value G great changes occur at low energies but then it remains nearly constant.
For the „pseudo-channel-cut" mode the beam shift is critical at low energies. This will be discussed in detail in section 4.5.3.

From the estimation of the motions R and G it was specified to restrict the R-range to 120 mm in order to make sure that the motion gives no additional mis-setting of the second crystal. This results in a restriction of the useable upper energy for the Si(111) crystals just below 30 keV. On the other hand at this energy the footprint of the incoming beam on the first crystal covers the whole length of the crystal. An extension of the energy range above 30 keV for the Si(111) demands a larger crystal which causes conflicts with the geometrical crystal arrangement at low energies. However, this is not a strong limitation because the full energy range is useable with the Si(311) crystal set.

The layout of the monochromator mechanics is specified in such a way to have enough space for the insertion of a bending device for the second crystal at a later stage. The bending of the second crystal will perform the sagittal focussing as demanded in the design specifications. At present there are different technical solutions for bending devices under development and testing. In the moment it is to early to decide which is the best solution for the purposes of ROBL. The effects of sagittal focussing are studied by ray-tracing calculations which will be reported in chapter 5.

4.5.2. Analytical Calculation of the Resolution

In this section the energy resolution is calculated from analytical expressions. The results from ray-tracing calculations will be reported in chapter 5.

The energy resolution of a crystal monochromator is a function of the width of the crystal reflection and the divergence of the incident beam. The width of a reflection is dominated by the mosaic spread for an imperfect crystal, but is equal to the intrinsic (Darwin) width of the Bragg reflection for a perfect crystal [4.9].
The energy band-pass through a monochromator is given by :

$$\Delta E/E = \cot \theta_m \; [\omega_D^2 + \Phi^2]^{1/2} \qquad (4.11)$$

where θ_m is the Bragg angle on the monochromator, ω_D is the Darwin width of the crystal and Φ is the vertical divergence of the radiation [4.6].
For the calculation of the resolution the full width at half maximum of Φ has to be used. This is already calculated in equ. (4.8) and given in Table 4.5 with the abbreviation FWHM.

The Darwin width is proportional to the structure factor and given by [4.9]

$$\omega_D=(2/\sin 2\theta)\,(r_e\lambda^2/(\pi V_{cell}))\;P\,|F_{hr}|\,\exp(-M) \qquad (4.12)$$

$$\omega_D=(4\,r_e\,d^2)/(\pi V_{cell})\,P\,|F_{hr}|\,\exp(-M)\,\tan\theta \qquad (4.12\,a)$$

where P is the Polarization factor, exp(-M) the temperature factor correlated with the Debye-Waller factor D = exp(-2M), F_{hr} is the structure amplitude of the crystal, V_{cell} the volume of the unit cell, d the lattice spacing, and r_e the Thomson electron scattering length.
In Table 4.7 the calculated energy dependence of the Darwin width and the Bragg angle are given for different reflections of silicon.

Table 4.7: Energy dependence of the Bragg angle and the Darwin width of different reflections of silicon.

	E (keV)	5	10	15	20	25	30	35
	θ (rad)	0.40519	0.19840	0.13183	0.09871	0.07893	0.06575	0.05634
(111)	ω_D^{nc} (mrad)	0.06224	0.02917	0.01924	0.01437	0.01148	0.00955	0.00818
	θ (rad)	0.70177	0.32875	0.21693	0.16214	0.12950	0.10784	0.09237
(220)	ω_D^{nc} (mrad)	0.05213	0.02104	0.01359	0.01009	0.00803	0.00668	0.00571
	θ (rad)	0.85863	0.38825	0.25513	0.19043	0.15200	0.12654	0.10836
(311)	ω_D^{nc} (mrad)	0.03478	0.01228	0.00783	0.00579	0.00460	0.00382	0.00326

For a divergence $\Delta\theta$, expressed in radians, differentiation of the Bragg equation leads to

$$\Delta E/E=\Delta\lambda/\lambda=\Delta\theta\,\cot\theta. \qquad (4.13)$$

This is equivalent to equ. (4.11).

Substitution of ω_D for $\Delta\theta$ gives for the intrinsic resolution of the perfect crystal and including the cotθ gives according to equ. (4.12a) a constant contribution I_1 to the resolution. In the cases discussed we get $I_1^{Si(111)}=0.1421$ mrad, $I_1^{Si(220)}=0.06167$ mrad, and $I_1^{Si(3111)}=0.0300$ mrad.
The fractional energy resolution of a perfect crystal is independent of the photon energy and proportional to the structure factor. However, the energy resolution of

the reflected beam can be modified by using *asymmetrically cut* crystals, with diffracting planes inclined to the crystal face.

The true resolution in the beam is a convolution of the intrinsic resolution of the monochromator crystal and the resolution I_2 due to the divergence of the incident beam.

$$(\Delta E/E)_{total}=(I_1^2+I_2^2)^{1/2} \qquad (4.14)$$

I_2 has to be calculated from FWHM of Table 4.5 multiplied by cotθ. Unlike the intrinsic part I_1, the part via I_2 is dependent on the photon energy selected, and on the storage ring parameters. The calculated data for $(\Delta E/E)_{total}$ are given in Table 4.8 The energy dependence of the energy resolution of a silicon monochromator with the natural divergence of the synchrotron beam is shown in Fig 4.8. The energy width of the absorption edges of the elements is indicated additionally.

Table 4.8: Energy resolution calculated for different reflecting planes of the monochromator with the natural divergence of the source.

	E (keV)	5	10	15	20	25	30	35
Si (111)	I_2 (10^{-3})	0.4785	0.7606	0.9711	1.1503	1.3101	1.4563	1.5921
I_1= 0.1421	$(\Delta E/E)_{tot}$ (10^{-3})	0.49917	0.77380	0.98149	1.15901	1.31775	1.46317	1.59848
	ΔE (eV)	2.496	7.7380	14.722	23.180	32.944	43.895	55.947
Si (220)	I_2 (10^{-3})	0.2446	0.4497	0.5858	0.6985	0.7980	0.8885	0.9723
I_1= 0.06167	$(\Delta E/E)_{tot}$ (10^{-3})	0.25227	0.45394	0.58909	0.70126	0.80037	0.89062	0.97429
	ΔE (eV)	1.261	4.539	8.8360	14.025	20.009	26.719	34.100
Si (311)	I_2 (10^{-3})	0.1806	0.3751	0.4951	0.5928	0.6784	0.7561	0.8279
I_1= 0.030	$(\Delta E/E)_{tot}$ (10^{-3})	0.18309	0.37632	0.49599	0.59353	0.67907	0.75668	0.82848
	ΔE (eV)	0.915	3.763	7.440	11.871	16.977	22.701	28.997

As shown in Fig. 4.8 the required energy resolution for the EXAFS measurements can not be obtained from a low order reflection of a perfect silicon crystal. The energy resolution is in most cases greater than the natural energy width of the absorption edge. From Table 4.8 it follows, that the divergence of the source determines the resolution. The required resolution can be obtained by using a cylindrical mirror in front of the monochromator to collimate the beam vertically. After collimation the residual vertical divergence of the beam is determined by the finite size of the source. From the Charcteristics of the bending magnet source [4.10] a FWHM source size (s_{hor} x s_{vert}) of 440 x 300 μm^2 gives at the position of the first mirror in a distance of x_{m1}= 26 m a divergence of

$$\alpha = \tan^{-1}(s_{vert}/ x_{m1}) \quad = 11.5\ \mu rad \qquad (4.15)$$

The calculated resolution for different reflecting planes od silicon single crystals is compiled in Table 4.9 and shown in Fig. 4.9.* The resolution is now comparable or better than the natural energy width of the absorption edges. Only the use of a collimating mirror allows to achieve the resolution required for XAS-experiments.

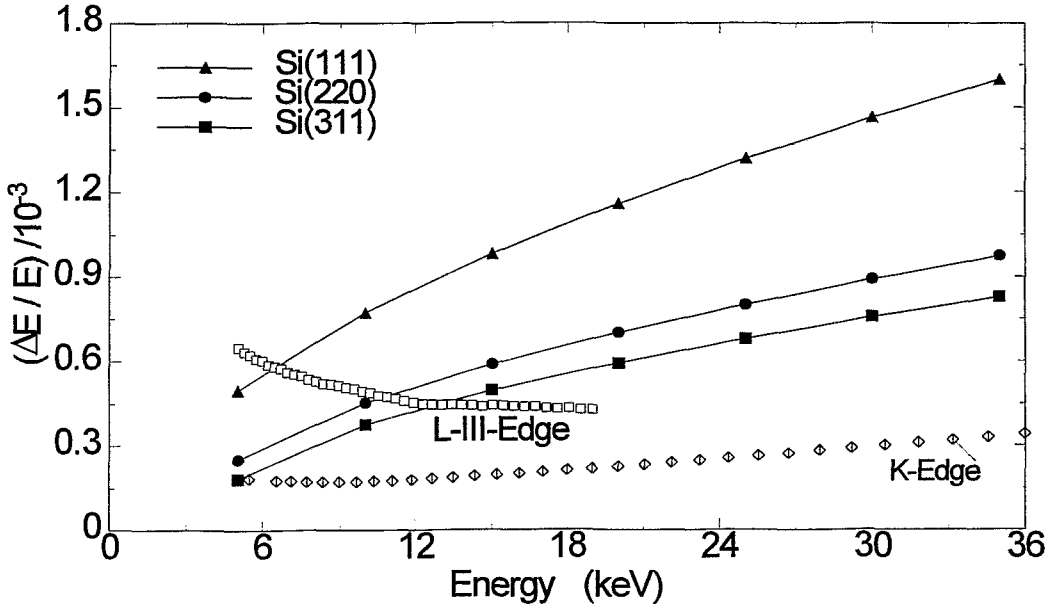

Fig. 4.8: Calculated energy resolution of only the monochromator of silicon crystals with different reflecting planes in dependence on energy. For comparison the natural line width of absorption edges of the elements is indicated.

Table 4.9: Energy resolution calculated for different reflecting planes of the monochromator with a collimating mirror in front of the monochromator.

	E (keV)	5	10	15	20	25	30	35
Si (111)	I_2 (10^{-3})	0.0268	0.0572	0.0868	0.1162	0.1454	0.1747	0.2039
I_1= 0.1421	$(\Delta E/E)_{tot}$ (10^{-3})	0.1446	0.1532	0.1665	0.1835	0.2034	0.2252	0.2486
	ΔE (eV)	0.723	1.532	2.498	3.671	5.084	6.756	8.700
Si (220)	I_2 (10^{-3})	0.0136	0.0338	0.0524	0.0705	0.0886	0.1066	0.1245
I_1= 0.06167	$(\Delta E/E)_{tot}$ (10^{-3})	0.0632	0.0703	0.0809	0.0937	0.1080	0.1232	0.1390
	ΔE (eV)	0.316	0.703	1.213	1.874	2.699	3.694	4.864
Si (311)	I_2 (10^{-3})	0.0100	0.0282	0.0442	0.0599	0.0753	0.0907	0.1061
I_1= 0.03004	$(\Delta E/E)_{tot}$ (10^{-3})	0.0316	0.0412	0.0535	0.0670	0.0811	0.0956	0.1102
	ΔE (eV)	0.158	0.412	0.802	1.339	2.027	2.866	3.858

* It should be noted, that the source size parameters used for the calculations were given for 10% coupling in the storage ring. The latest data from ESRF used only 2% coupling (Beamline Handbook, December 1995). This results in a source size of 280x110 μm^2. Our calculation is than a conservative estimation of the resolution. But the same source parameters will used for the ray-tracing calculations.

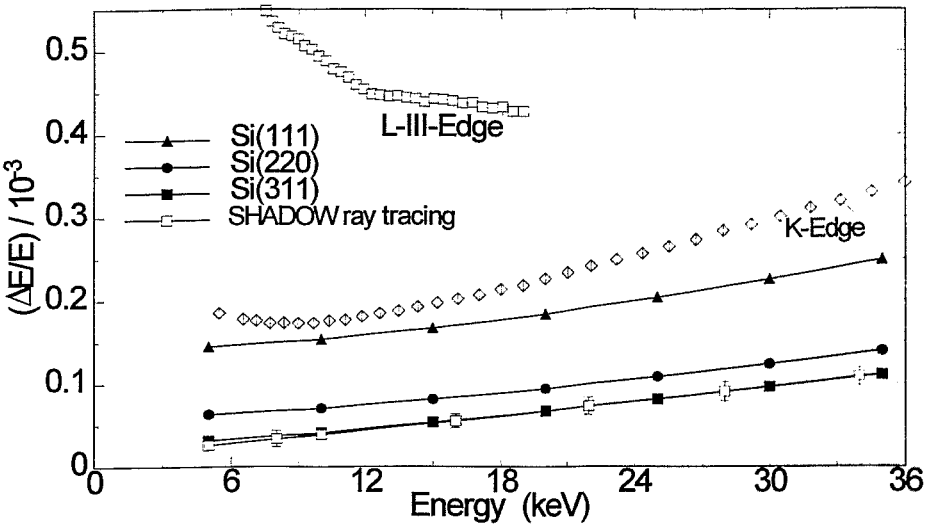

Fig. 4.9: Calculated energy resolution of the monochromator of silicon crystals for different reflecting planes in dependence on energy. A collimating mirror in front of the monochromator reduces the vertical divergence of the incident beam. For comparison the natural line width of absorption edges of the elements is indicated.

4.5.3. Beam Motion During QEXAFS-Scans

In the standard operation mode the monochromator will produce the outgoing beam always at the „fixed-exit" of 18 mm above the incident beam. In the Quick-EXAFS experiment an energy interval of typically 500 eV will be scanned in times of 100 seconds. In such short periods it is difficult to set the second crystal in the exact position by moving along R and G, respectively, according to Fig. 4.7. In order to save the setting time a so-called channel-cut mode is foreseen for the QEXAFS experiments. In this mode, the two crystals of the monochromator are set in the correct position for the starting energy of the scan. In the scan only the Bragg angle rotation (θ_1 of Fig. 4.7) is performed. This results in a violation of the fixed exit conditions and the outgoing beam moves. This high variation (deviation from ideal value of 18 mm) was calculated for the reflection planes Si(111) and Si(311), respectively. The beam shift is shown in Figs. 4.10 and 4.11. In both cases also the effect of correcting one translational position (G or R) during the scan is indicated.

It can be seen from the figures that the beam shift is significant (up to 33% of beam height) in the energy region below 10 keV. For higher energies the beam shift is only 10% of the vertical beam dimension. For a (partial) correction of the beam shift, the R translation during the scan is most effective. The curves marked with dhG in the Figs. 4.10 and 4.11 indicate that already above 8 keV the beam shift can be compensated by the simultaneous R-translation. Since R-translation

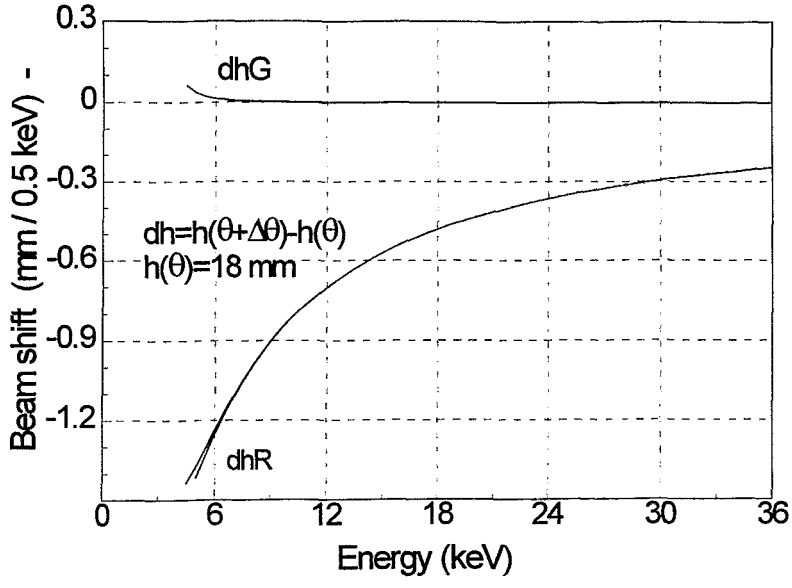

Fig. 4.10: Variation of the beam height dh=dh(E) relative to the standard beam shift of 18 mm at the exit of the double crystal monochromator for Si(111) crystals. The energy variation during the QEXAFS-scan is assumed to be ΔE=0.5 keV. dh is the variation for channel cut geometry (dG=dR=0). dhG is the variation if R-translation is performed during the scan (dG=0) and dhR if G-translation is performed (dR=0).

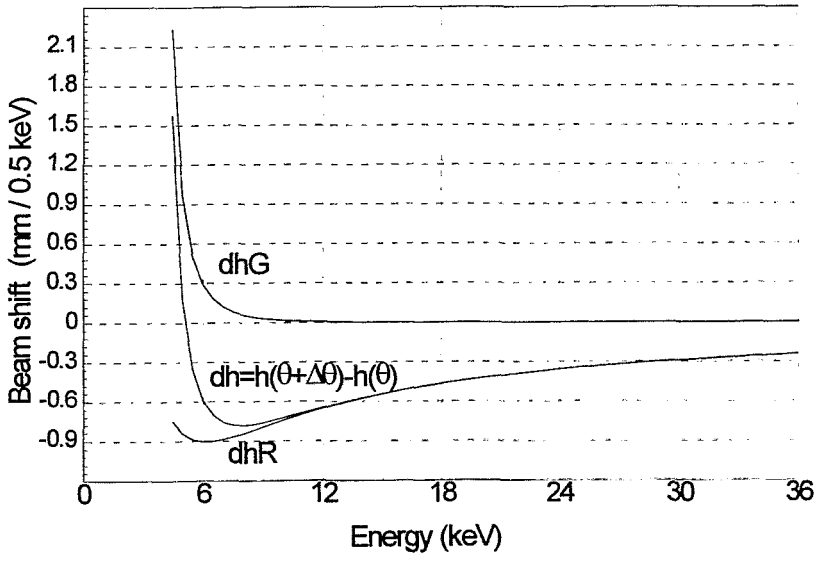

Fig. 4.11: Variation of the beam height dh=dh(E) relative to the standard beam shift of 18 mm at the exit of the double crystal monochromator for Si(311) crystals. The energy variation during the QEXAFS-scan is assumed to be ΔE=0.5 keV. dh is the variation for channel cut geometry (dG=dR=0). dhG is the variation if R-translation is performed during the scan (dG=0) and dhR if G-translation is performed (dR=0).

is a linear motion in dependence on energy it may be possible to use this in cases when a beam shift is not tolerable and when the velocity of the QEXAFS scan is moderate.

An additional point to be noted is the location of the monochromator between two mirrors. A beam shift at the monochromator exit causes a nonideal incoming beam on the second mirror. This results mainly in intensity reduction. The reduction factor IV can be approximately estimated by the geometrical configuration.

$$IV(E) = (q(e)-dh)/q(E) \qquad (4.16)$$

q(E) is the vertcal dimension of the beam. At low energy it is given by the acceptance height of the first mirror (3 mm). At higher energies it is slightly reduced by the smaller divergence of the primary beam.

In the case of a flat, non-focussing mirror the lowering of the beam from the monochromator causes an upward shift of the center of gravity of the reflected beam. Because of the nearly parallel beam produced by the first mirror the beam shift at the sample is the same as at the exit of the monochromator. In the case of a curved, focussing mirror behind the monochromator the beam will be focussed onto the sample. It is expected that the beam shift in the QEXAFS experiment does not significantly influence the focus position on the sample but the intensity.

4.6. Beam Defining and Diagnostic Elements

4.6.1. Overview

Besides the main components of the X-ray optics, the monochromator and the mirrors, there are various components located in the beam path from the ring wall down to the experimental end stations. The function of these components is the limitation of the beam in dimension and intensity as well as the diagnostics of the beam. There are slit units, a filter/attenuator unit, beam position monitors and a fluorescence screen. Moreover, there are components which separate the beam path in the vacuum from that in air, as the beryllium windows or terminate the beam at different positions within the beamline like the lead beam shutters.

For all the above mentioned components in the ROBL beamline either ESRF standard or in some CRG beamlines tested components are used.

4.6.2. Slit Units

In four positions of the beamline slit systems will be installed. Each system consists of two units for the horizontal and vertical limitation of the beam. The

systems are located in front of the first mirror, in front of the monochromator and in front of the experimental end-stations.

The slits will limit the beam to the dimension which is accepted by the optical components or which matches the sample dimension. Since the first two systems are exposed to the white synchrotron beam, these are cooled. The two slit systems near the experimental end-stations are only illuminated by a monochromatic beam, therefore cooling is not necessary.

The dimensions for the maximum opening of each unit are defined by the beam size. The horizontal size of the useable beam is limited by the acceptance of the mirrors to 3 mm. The maximum vertical size is given by the beam divergence and the distance from the source. Since the general concept implicates the use of a saggittally focussing second crystal in the monochromator, the beam has its maximum width at the monochromator position of 28.6 m. With a beam divergence of 2.8 mrad the maximum beam width is then about 80 mm.

For practical reasons the slit units for the limitation of the beam width are the same at all four positions, although the beam becomes narrower at the end-stations. The units defining the beam height are different in their dimensions.

Each slit unit consists of two independently moveable blades made from tungsten carbide. The movement of the blades is in different planes to allow a blade overlap for closing the beam. The main specifications of the slit units are:

- blade thickness: 6 mm
- radius of curvature of the beam defining edge of the blade: 5 mm $\pm$ 10 µm
- parallelism of the defining edges: 10 µm
- maximum opening for the width defining units: 100 mm
- maximum opening for the height defining units: 30 mm
- minimum overlap of blades: 6 mm
- positioning of the blades: by a stepper motor starting from a reference switch with a reproducebility of 1 µm
- resolution of the blade positioning: <10 µm
- minimum life time of each blade movement: 10^4 cycles

4.6.3. Filter / Attenuator

For some kinds of experiments it may be necessary to reduce the intensity of the primary beam. In order to facilitate this, an attenuator unit will be located in the beamline in front of the first mirror. In the ROBL beamline the ESRF standard design will be used.

The unit consists of two independently moveable racks. Each rack has 3 openings of 8 mm x 80 mm for the mounting of absorbing foils. The rack is cooled since the unit is exposed to the white beam. Each rack can be positioned to one of the three absorbers or fully out of the beam. The actual position is indicated be

switches. With this design one can use 6 different absorbers and 9 combinations of absorbers from the two racks.

The vacuum flange itself allows the installation of one additional rack at a later time.

4.6.4. Beam Diagnostic Elements

For the beam diagnostics four thin wire beam position monitors (BPM) and one fluorescence screen will be installed at ROBL. All components are standard designs of the ESRF.

The BPM allows a quantitative evaluation of the intensity distribution in the beam by scanning the wire across the beam and recording the induced current in the wire. The positions of the BPMs are: between the first mirror and the monochromator, behind the second mirror and in front of each end-station. The first three BPM have a single wire (type 70x3 modified to 80x3) while the last one is cross wired (type 40x3). In cases where the BPMs are located together with the slit systems they are in the same vacuum vessel and the relation between the limit switches of BPM and slit unit will be known for reference.

The critical specifications of the mechanics of the BPM are the parallelism of the wire to the horizontal plane (5 mm per meter) and the regularity of the linear speed while scanning the beam ($\pm$ 5%). The minimum life time of the wire movement is specified to 10^4 cycles.

The fluorescence screen will normally be installed behind the second mirror, i.e. after all components determining the monochromatic beam. Additionally, there will be an alternative position behind the mirror. In the working position the screen is oriented by an angle of 45° and will be observed by a CCD-camera. In the rest position the screen is swept out of the beam. The fluorescence screen allows a direct qualitative observation of the beam as a whole. It allows a quick information on the location and the form of the beam. The main application of the screen is a rough adjustment and the judgement on beam form deviations from the ideal rectangular form.

4.6.5. Influence of Beryllium Windows on Intensity

From the source point to the experiment the synchrotron radiation beam has to pass several beryllium windows. The first one of 0.5 mm thickness separates the storage ring from the beamline. Other beryllium windows in the beamline separate the vacuum from the atmosphere. Such positions are in front and behind the radiochemistry experiment and in front of the materials science end-station. Additionally two beryllium windows are located in front of and behind the monochromator to allow the change of the crystal pair while not breaking the

vacuum for other parts of the optics. This is important especially for the mirrors, since the coated surface is sensitive against contamination.

All beryllium windows in the beamline are specified to a thickness of 0.2 mm. In the low energy region of radiation there is a markable absorption effect of the beryllium windows. This effect was calculated for different thicknesses starting from experimental values for the transmission coefficient of a 0.5 mm beryllium window of CF 60 grade [4.11]. Fig. 4.12 shows the calculated transmission for two

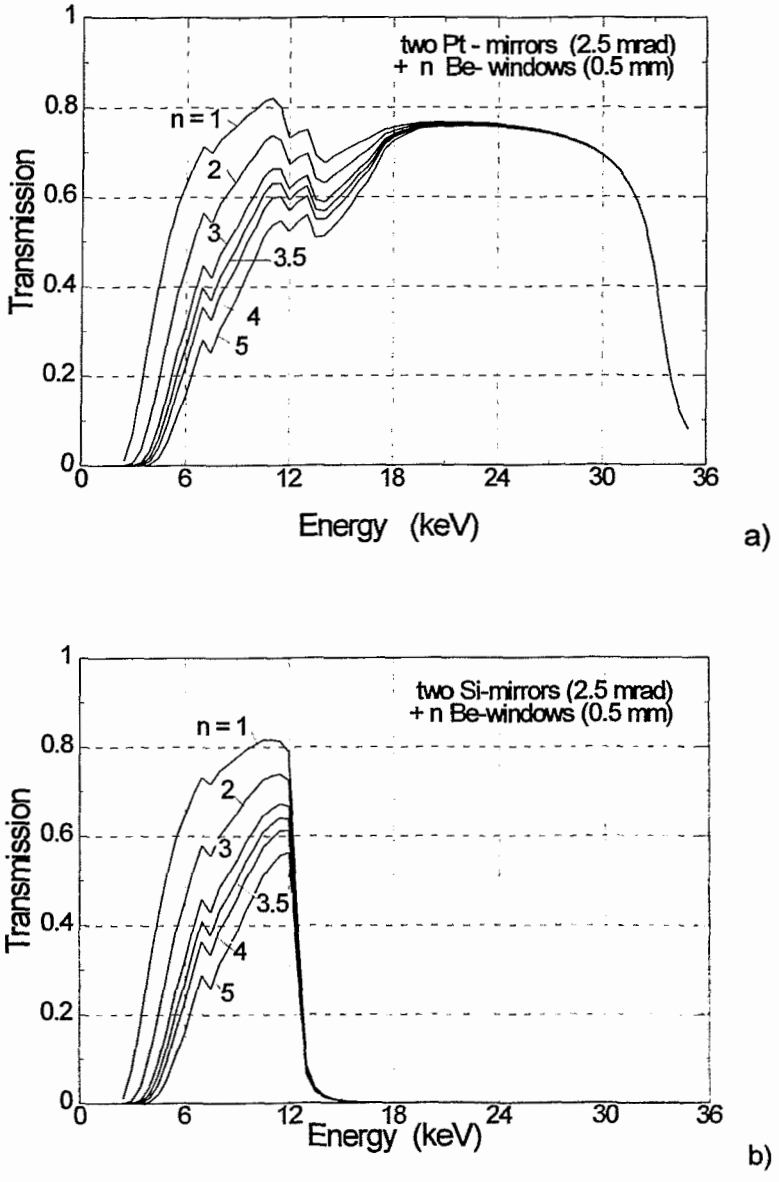

Fig. 4.12: Calculated transmission of two mirrors coated with platinum (a) and with silicon (b) and beryllium windows of different thickness in dependence on energy. The absorption of a beryllium windows of 0.5 mm thickness was experimentally determined for CF 60 grade beryllium [4.11]. The parameter n is the cumulative thickness of Be windows as nx0.5 mm.

mirrors either from platinum or from silicon and a different number of beryllium windows with a overall thickness of nx0.5 mm. This combination was choosen, since it represents the energy dependence of the available spectrum on the sample.

The case n = 1 represents the situation when only the ring Be window is installed. The standard situation for the radiochemistry experiment is slightly below the curve n = 2. In the beamline are 3 windows summing up to 0.6 mm beryllium. For the materials science experiments one can have the situation n = 3, i.e. all beryllium windows are installed. For experiments which need the low energy part of the spectrum there is the possibility to remove the two Be windows in the radiochemistry hutch and close the vacuum tube in this section as well as to remove the last Be window in front of the sample. It is understood that in such a case the sample is also in a vacuum chamber. This configuration equals a beryllium thickness of 0.9 mm and is represented by an intensity distribution slightly higher than the curve for n = 2 in Fig. 4.12 . The intensity gain at 6 keV compared with the configuration of all Be windows in place is as much as 50%. This is the reason for the option of removing the beryllium windows in the radiochemistry hutch which are installed mainly for safety reasons.

5. Resolution, Focussing and Intensity (Ray Tracing Calculations)

For the ray-tracing, we used the SHADOW software package developed by F.Cerrina et al. [5.1; 5.2]. The program is designed to provide an optimal simulation of instruments at synchrotron radiation sources.

As briefly described in [5.3], SHADOW computes the propagation of a photon beam through an optical system. The beam is a collection of rays in a given point of the beamline which are stored in a disk file. The optical system (OS) is a collection of optical elements (OEs) (mirrors, multilayers, slits, screens etc.) placed in a sequential order. The OS of ROBL,.containing 4 OEs, is described in section 4.2. Each ray is an array of variables of special physical meaning. The first six defines the geometry: spatial coordinates (x,y,z) and the directions of the ray (x',y',z'). The rest of the columns defines the history of the ray traversing the OS (electric vector for s-polarization and p-polarization, flag for lost ray, wavelength)

The source is the beam at the starting point. It is generated by SHADOW by sampling the spatial, angular, energy and other qualities of the synchrotron radiation sources (i.e., bending magnets, wigglers and undulators) into a finite number of rays, using Monte Carlo method. The here used parameters for the bending magnet source of ROBL are described in section 4.3. At the source position the intensity of each ray (or better, its probability of observation) is set to 1. This intensity will decrease along the beamline because of the interaction of the ray with the OEs. The source generated by SHADOW samples linearly the real source, which allows to scale the intensity with the number of photons.

SHADOW traces the source sequentially through each OE of the OS. SHADOW solves the intercept of each ray at a given OE, calculates the output direction and the decrease in intensity. The decrease is calculated for each ray using a physical model (i.e. Fresnel equations for mirrors, dynamical theory of the diffraction for a perfect crystal, etc.)

5.1. Resolution

The resolution was calculated with SHADOW code for the full design characteristics of the beamline. These are the distances, the orientation, and the material properties of the optical elements.The Be-windows are taken into account as absorbing screens between these elements.The dependence of resolution $\Delta E/E$ on energy for Si(311) and Si(111) double crystal monochromators is shown in Figs. 5.1 and 5.2. The resolution was calculated for both cases of reflecting surfaces of the mirrors.

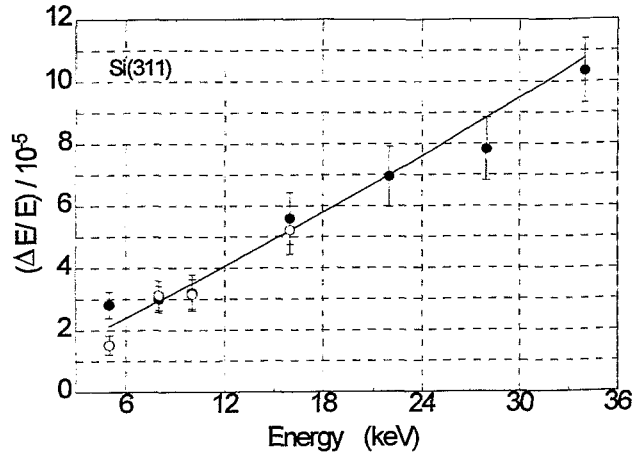

Fig. 5.1: SHADOW simulation results of the dependence of resolution ΔE/E on energy for Si(311) (Filled circles:Pt- mirrors; open circles: Si-mirrors)

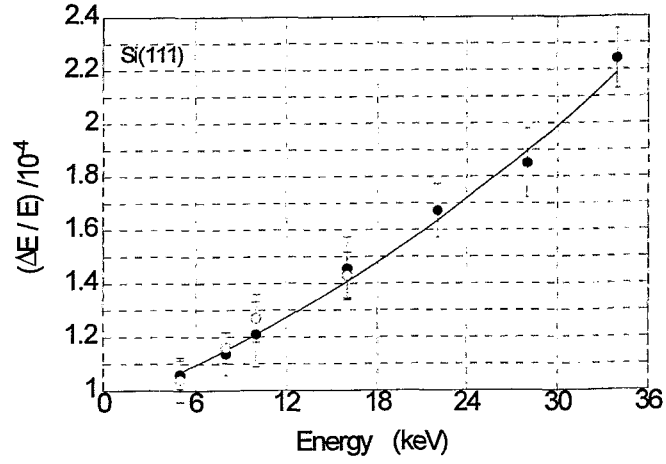

Fig. 5.2: SHADOW simulation results of the dependence of resolution ΔE/E on energy for Si(111) (Filled circles:Pt- mirrors; open circles: Si-mirrors)

Within the statistical errors of the modelling the resolution is, as expected, not influenced by the type of the mirrors's reflecting surface. Compared with the pure analytical calculation (Fig. 4.9) the ray-tracing calculations gives 10 - 15% better resolution values. Thus the analytical values are a good estimate for the resolution.

5.2. Focussing and Spot Size

5.2.1. Sagittal Focussing Conditions

The monochromator is formed by two perfect Si crystals in the (+n,-n) configuration, diffracting in the plane perpendicular to the electron orbit. The first crystal is flat, while the second one is bent so as to assume a cylindrical shape

with axis parallel to the beam direction. This geometry will focus the beam out of the plane of scattering (sagittal focussing), i.e. in the horizontal plane in the present case. The following relation holds for sagittal focussing:

$$1/p_h + 1/q_h = 2 \cdot \sin\theta / R_{sag} \qquad (5.1)$$

where R_{sag} is the radius of curvature, θ the Bragg angle, and p_h and q_h are the source and image distances, respectively. To keep the focus fixed at constant distance (sample position) from the curved crystal as the photon energy varies, the curvature R_{sag} will be varied. The values of R_{sag} for focussing at the experimental positions E1and E2 as well as for making the beam (horizontally) parallel (F_∞) are shown in Fig. 5.3 for Si(311) and Si(111) , in dependence on energy .

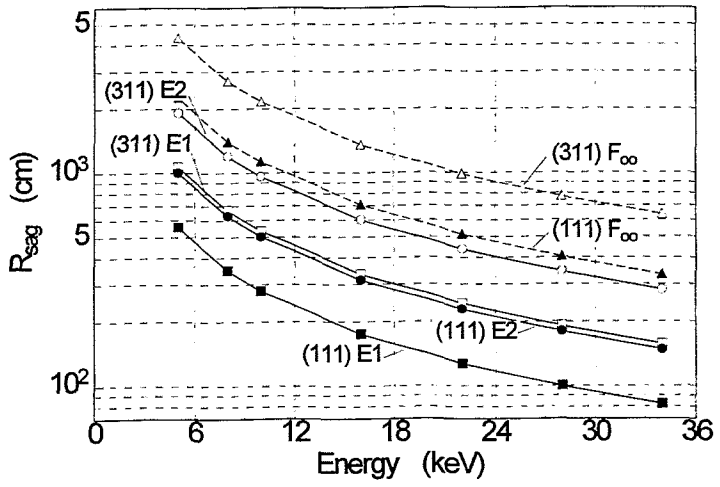

Fig.5.3: Sagittal focussing radius R_{sag} versus energy for the two focal points E1, E2, and for making the beam (horizontally) parallel (F_∞) for a Si(311) and a Si(111) monochromator crystal set, respectively.

The ideal geometry for a point-to-point focussing X-ray monochromator is one in which the reflecting planes are curved to confocal ellipsoids of revolution and the surface ground to the Rowland circle . In the monochromator this ideal crystal shape is approximated by a cylinder. Therefore, due to the horizontal divergence ϕ of the beam, only the rays impinging on the axis of the cylinder (ϕ=0) have the correct Bragg angle defined by the first crystal. Those being diffracted off axis ($\phi \neq 0$) will have an angle θ which differs from the Bragg condition by a quantiy $\Delta\theta = \theta - \theta_B$, which is a function of ϕ. As long as $\Delta\theta$ remains smaller than the total width of the reflection curve (Darwin width or rocking curve width) the rays will be diffracted by the double crystal system, otherwise they will not be diffracted and there will be a loss in intensity [5.4].

Rocking curves of the Si(311) and Si(111) planes were calculated with the SHADOW code for different energies as shown in Figs. 5.4 and 5.5. For small

Bragg angles the values of θ are found to be independent of the horizontal divergence ϕ only when the demagnification m_h is close to 1/3 [5.4]. In this geometry there is no loss of intensity associated with the mismatch in the Bragg angles between the first and the second crystal. For ROBL in the first hutch (E1 at 38 m from the source point) with

$$m_h{}^1=q_{h1}/p_{h1}=9.5/28.7=0.331 \qquad (5.2)$$

this condition is fulfilled.

The radiochemistry experiment was located at this position, since it requests the minimal spot size On the other hand the experimental programe is oriented towards the higher energy band pass > 15 keV. For these energies the Rocking curves becomes narrower (c.f. Figs. 5.4 and 5.5). So it is essential that the configuration is not sensitive on the above discussed Bragg angle mismatch.

In general, the intensity loss caused by the crystal's curvature raises with increasing energy because of the decrease of the useful horizontal acceptance $\Delta\phi$.

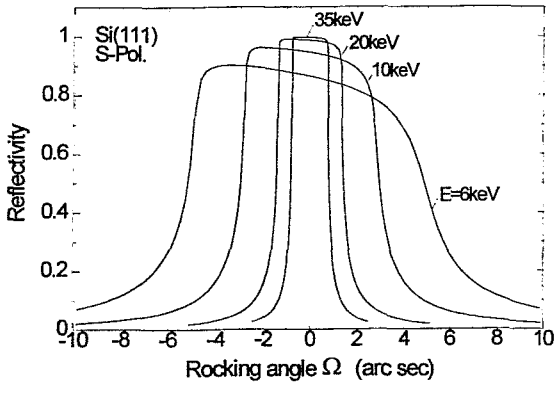

Fig. 5.4:
Rocking curves(s-polarization) of Si(111) calculated for four different energies

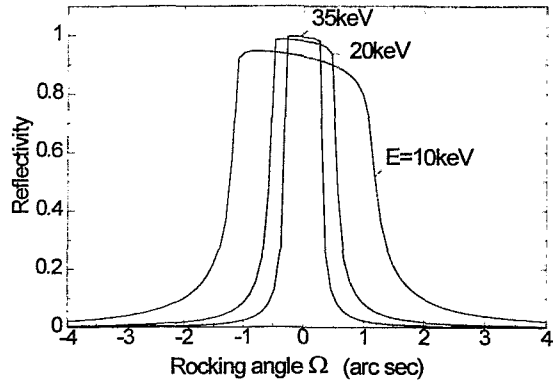

Fig. 5.5:
Rocking curves(s-polarization) of Si(311) calculated for three different energies

It is important to note that, concerning the loss of intensity caused by the crystal, curvature, the higher the energy, the lower the useful horizontal aceptance $\Delta\phi$.

The sensitivity of the spot size on the sagittal focussing condition for Si(311) crystals is shown in Figs. 5.6 , 5.7 and 5.8 for the various experimental positions and different energies. It can be seen that the horizontal spot size Δx is very sensitive to the accurate radius of curvature of the crystal. The size can vary by one order of magnitude for a change of only 4 cm in R_{sag} as to see at the inserted curve in the Fig. 5.6. This result shows the high demands on the stability of the bending radius for maximal focussing (minimal spot size Δx)

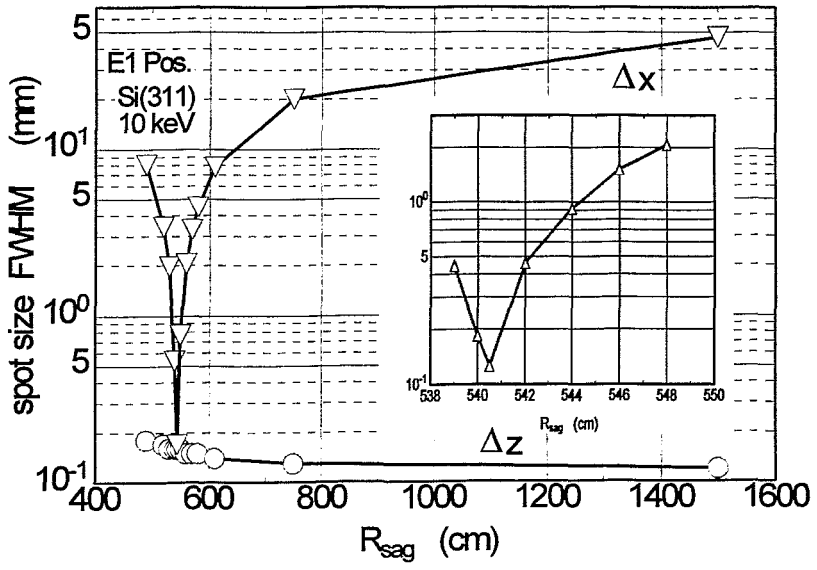

Fig. 5.6: SHADOW simulation results of spot size FWHM-values Δx and Δz on sagittal bending radius R_{sag} for E = 10 keV at position E1. The inserted diagram shows the region of minimal Δx size on an enlarged scale.

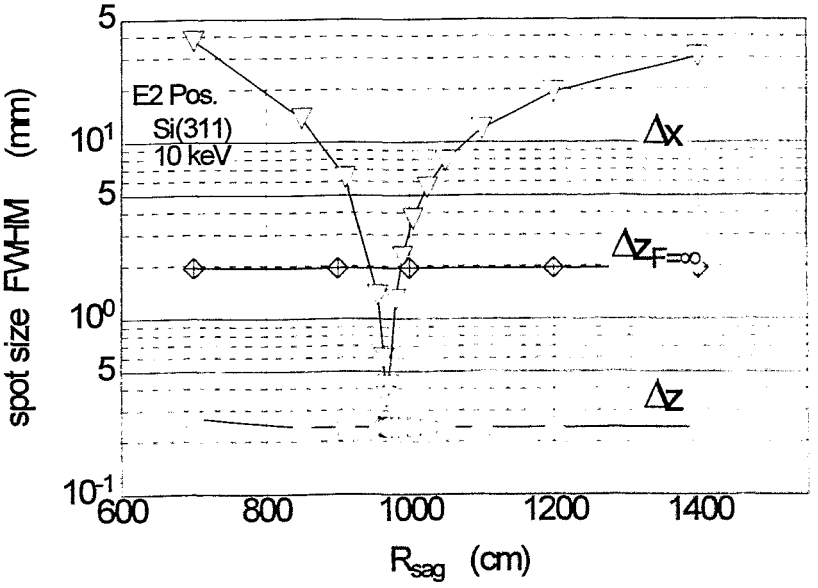

Fig. 5.7: SHADOW simulation results of spot size FWHM-values Δx and Δz on sagittal bending radius R_{sag} for E = 10 keV at position E2. For comparison $\Delta z_{F=\infty}$ indicates the spot size Δz of a vertically parallel beam (reached by of M2).

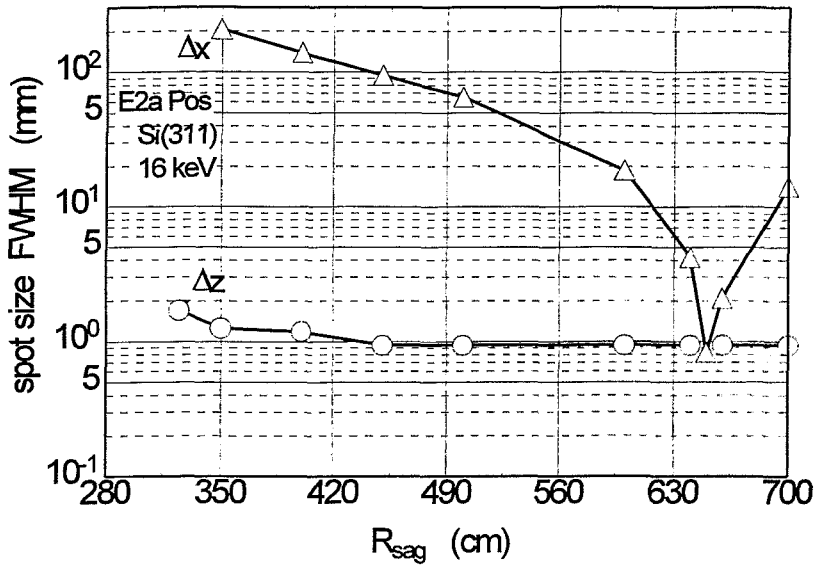

Fig. 5.8: SHADOW simulation results of spot size FWHM-values Δx and Δz on sagittal bending radius R_{sag} for E = 16 keV at position E2a.

5.2.2. Horizontal Demagnification

It is only the monochromator that determines the horizontal dimensions of the image. In absence of sagittal focussing *aberrations*, the horizontal dimension Δx_i in the focal spot is:

$$\Delta x = m_h \cdot \Delta x_s \qquad (5.3)$$

where Δx_s is the horizontal dimension of the source and m_h is the horizontal demagnification. This contribution to the spot size will have a Gaussian profile. Table 5.1 gives the values of m_h for the three focal planes E1, E2 and E2a .

Table 5.1: Horizontal demagnification at the three sample positions of ROBL

	E1	E2	E2a
m_h	0.331	0.801	0.899

5.2.3. Vertical Demagnification Due to the Focussing Mirror

Since both transmission and resolution are maximized by reducing the divergence of the beam on the monochromator, mirror M1 transforms the diverging rays into a quasi-parallel beam, and mirror M2 focusses the monochromatic beam onto the image planes. The vertical demagnification is given by the ratio of the distance between the source and the mirror M1. The focussing parameters are listed in Table 5.2.

Table 5.2: Focussing parameters: p_v- distance from source to M1; q_v - distance from image to M2; $m_v = q_v/p_v$ - vertical demaginfication

exp. position	p_v (m)	q_v (m)	m_v
E1	26	7.2	0.277
E2	26	20.7	0.796
E3	26	23.5	0.904

We will estimate the curvature of the mirrors in the cylindrical approximation, where the ideally parabolic or elliptical surface needed is substituted by a cylinder of radius R_{mer}. In this approximation, the relation between R_{mer}, the source and image distances p_v and q_v an the incidence angle α_i is:

$$1/ p_v + 1/ q_v = 2/ R_{mer} \sin\alpha_i. \qquad (5.4)$$

In order to obtain high resolution with a minimum loss of intensity it is necessary to reduce the vertical divergence of the rays of impinging on the first crystal of the monochromator as much as possible; this is accomplished by adopting a collimating profile for M_1. A mirror in the form of a paraboloid of revolution with axes parallel to the $\psi = \varphi = 0$ directions converts a photon beam coming from a point source situated in its focus into a parallel beam. The vertical divergence of the photon beam after the mirror , $\Delta\psi_o$, is only due to the source vertical dimensions σ_z. In the case of an ESRF bending magnet beamline:

$$\Delta\psi_o = 2.35 \cdot \sigma_z / p_{M1} \approx 12\ \mu\text{rad} = 2.5\ \text{arc sec}. \qquad (5.5)$$

This value of intrinsic divergence implies that spurious slope errors on the mirrors (e.g. manufacturing errors and heat load distorsions) should ideally be not greater than a few (1 - 2) arc seconds.
In the cylindrical approximation an estimate of the radius of curvature of M_1 is obtained by going with q_v to infinity.

$$R_{mer}^{M1}\ (\text{m}) = p_{M1}\ (2 / \sin\alpha_i). \qquad (5.6)$$

We get with $\sin\alpha_i \approx 2.5 \cdot 10^{-3}$: $R_{mer}^{M1}\ (\text{m}) \approx 20.8$ km

Table 5.3 shows the geometric parameters of the first mirror, M1.

Table 5.3: Mirror M1 (Pt and Si strips on the surface)

incidence angle α_i (mrad)	length L (mm)	width H (mm]	radius R_{mer}^{M1} (km)	vertical acceptance $\Delta\psi$ (μrad)	exit vertical divergence $\Delta\psi$ (μrad)
2.5	1200	2 x 75	20.80	115	12

The second mirror M2 at about 31 m from the source point, vertically focusses the quasi-parallel monochromatic beam on the three sample positions. The curvatures R_i^{M2} for M2 are obtained for p_{M2} going to infinity. Table 5.4 contains information on the bending radii of M2.

Table 5.4: Mirror M2 (Pt and Si strips on the surface)

incidence angle α_i (mrad)	length L (mm)	width H (mm)	E1 R_1^{M2} (km)	E2 R_2^{M2} (km)	E2a R_{2a}^{M2} (km)
2.5	1200	2 x 75	5.76	16.56	18.80

The vertical dimension in the image points E_i is determined by the vertical demagnification m_v^i, the spherical aberations δ_v^i, and the sagittal focussing *aberation* induced by the monochromator. The smallest spot size is obtained for an optimum value of m_v (m^v_{opt}) for which the sum of the several above mentioned contributions is minimized [5.5]. It depends on the vertical divergence of the beam on the mirror, on the source size and the distance of the source from the mirror. In the case of ROBL one obtains $0.5 \leq m^v_{opt} \leq 0.6$ which is in sufficient agreement at position E2.

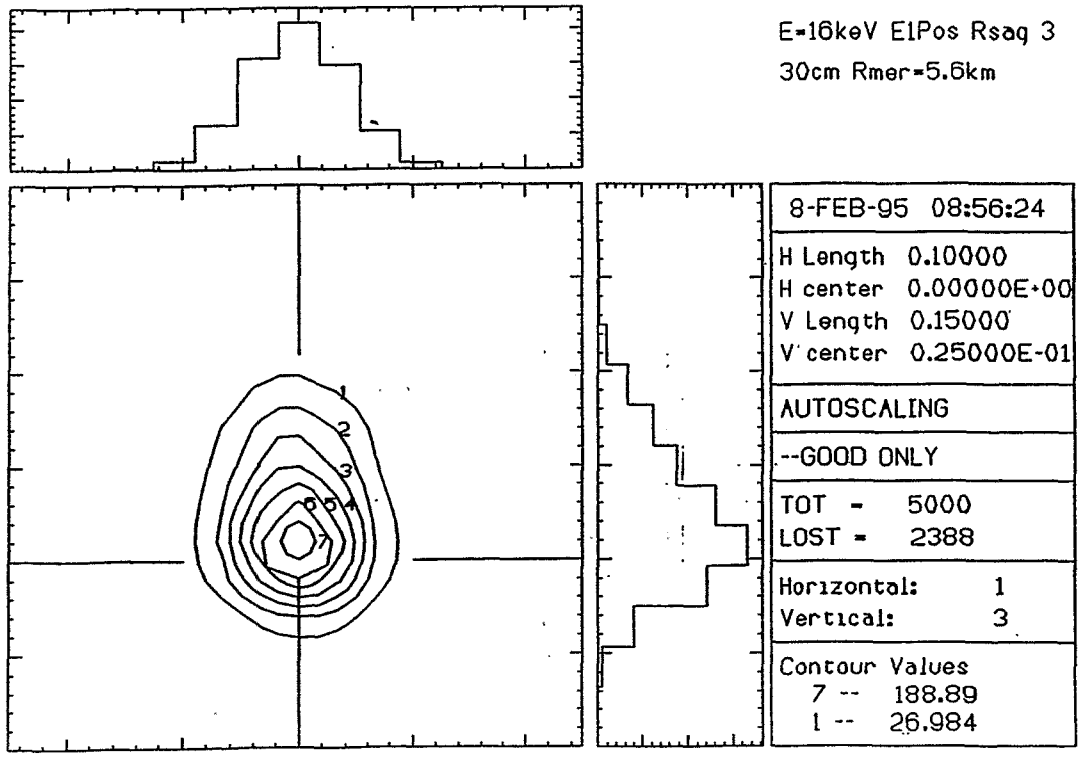

Fig. 5.9: xz-contour plot of a beam focussed at the image plane in the experimental position E1 for Si(311) with E=16 keV, $R_{mer}=R_1^{M2}$ = 5.76 km, and R_{sag} = 338 cm (horizontal and vertical scale length are 0.1 cm (!) and 0.15 cm (!), respectively)

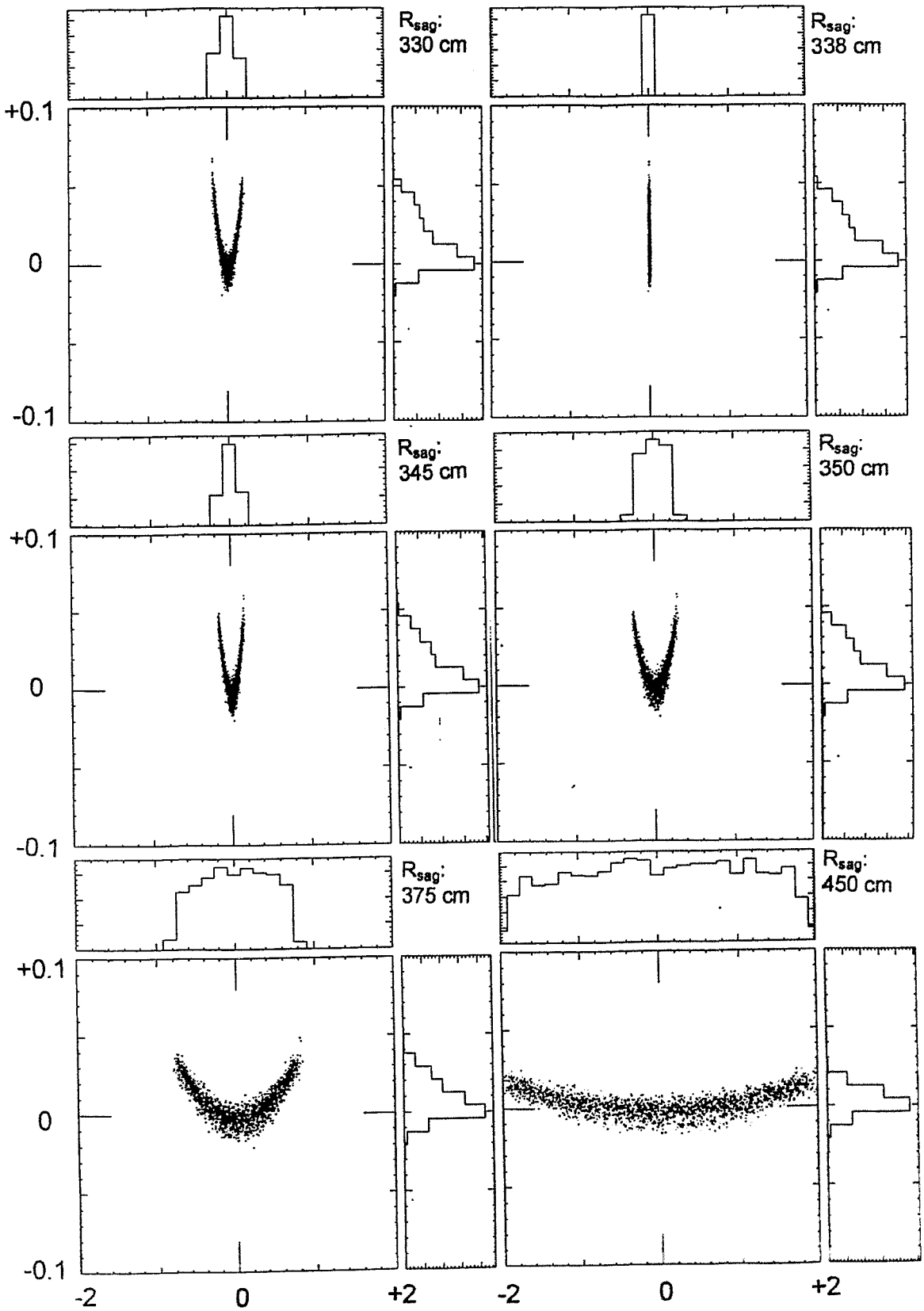

Fig. 5.10: Change of spot size at experimemtal position E1 with variation of the sagittal focussing radius R_{sag} for constant meridional focussing (R_{mer} = 5.76 km) at the energy E=16 keV. Units of the horizontal and vertical scale are centimeters. Note the different scales of both axes.

As an illustration of the influence of focussing beam profiles are shown for E=16 keV and E1 position in Figs. 5.9 and 5.10,. The contour or scattered plots are taken directly from graphical output (PLOTXY) of the SHADOW code. In Fig. 5.9 the beam profile is shown for proper focussing conditions. There is only a slight vertical asymmetry of the beam (due to spherical aberration) but otherwize the maximal focussing is achieved. Fig. 5.10 demonstrates the changes in the beam profile when R_{sag} is varried around the ideal value. From this profile variation the sensitivity of the spot size (Figs. 5.6 to 5.8) on sagittal bending radius can be understood.

5.2.4. Energy Dependence of Spot Size for the Positions E1 and E2

With the SHADOW code one is able to quantify the influence of the different types of aberrations on the beam size. The aberrations comes in due to the above discussed approximation of the bent mirror surfaces and the sagittaly bent crystal plane by spherical bent cylinder planes.

Whereas for various energies the spot size Δz is modified by these effects only, for Δx additional inaccuracies are introduced with the determination of R_{sag}. Due to this approximation the calculated value (Equ. 5.1) gives not exactly the minimal size. The latter one gets only from time consuming fine tuning calculations (results are given in Figs.5.6 to 5.8). Nevertheless, for estimations of the energy dependence only, in the following the rough values have been used.

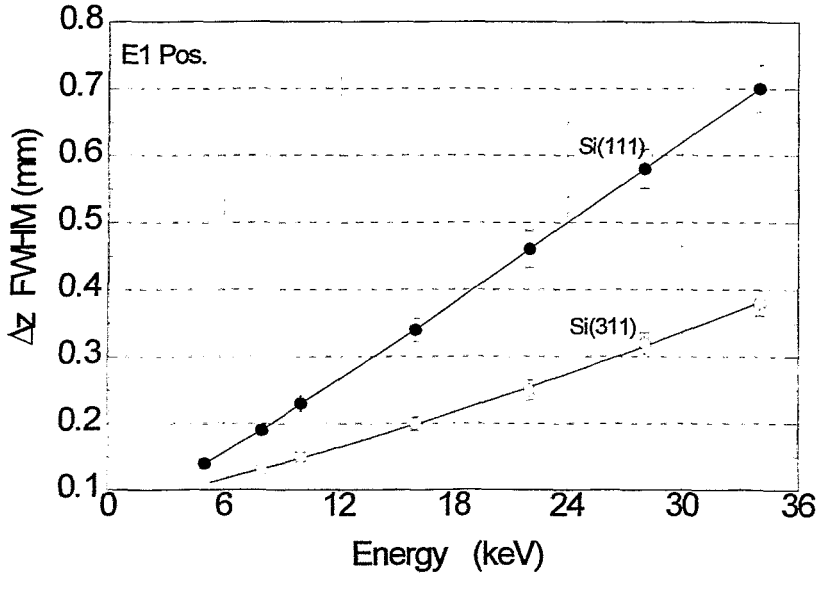

Fig. 5.11: Dependence of the FWHM-value of the spot size Δz on energy for Si(111) and Si(311) at experimental position E1.

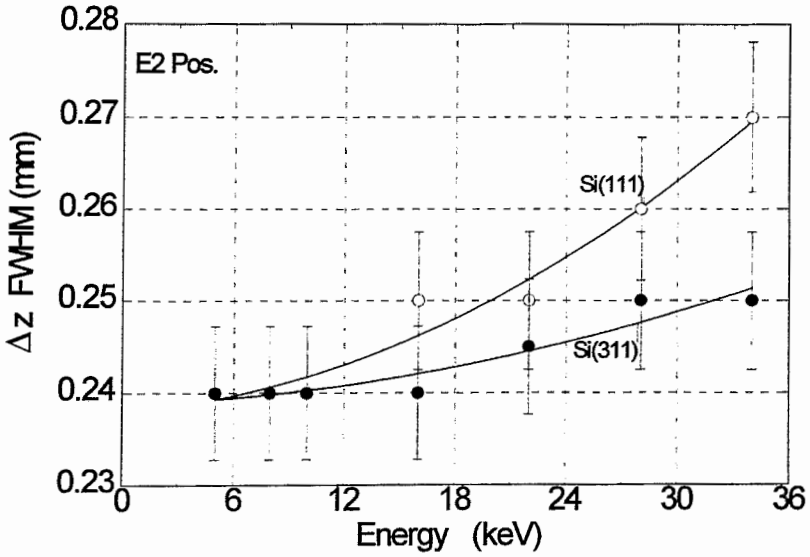

Fig.5.12: Dependence of the FWHM-value of the spot size Δz on energy for Si(111) and Si(311) at experimental position E2.

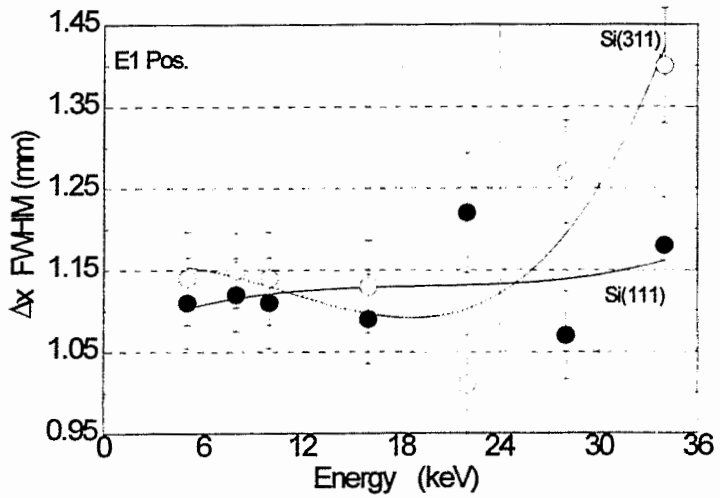

Fig. 5.13: Dependence of the FWHM-value of the spot size Δx on energy for Si(111) and Si(311) at experimental position E1. The values are determined for the calculated value of R_{sag} only and without fine tuning of R_{sag} they are not the minimal ones.

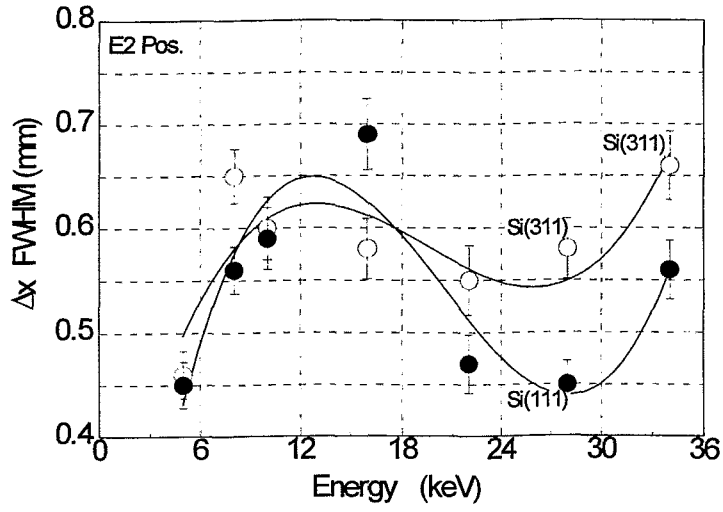

Fig. 5.14: Dependence of the FWHM-value of the spot size Δx on energy for Si(111) and Si(311) at experimental position E2. The values are determined for the calculated value of R_{sag} only and without fine tuning of R_{sag} they are not the minimal ones.

For Si(111) as well as Si(311) the energy dependence of the FWHM-values of the spot size Δz and Δx is shown in the Figs. 5.11 & 5.12 and Figs. 5.13 & 5.14 for the sample positions E1 and E2, respectively. The spot size Δz increases smoothly with energy. At E2 position, however, the spot size Δx is found to be enlarged also in the middle of the energy range of ROBL.

5.3. Intensity Estimations

5.3.1 Simulation of the Transmitted Photon Intensity

For an estimation of the photon flux at the image plane the energy distribution of the rays used in the ray tracing code SHADOW must be related to the photon flux emitted for the bending magnet source. Because in the estimate no any external influences (as additional absorption and scattering processes) were considered, the number of photons/sec behind the last Be-window is preserved. However, the photon flux at the sample (#/sec·mm^2), which is determined by the spot size (or beam size), is sligthly different for the three experimental positions due to the given focussing conditions.

The below given results are calculated *without* including roughness and slope errors of mirrors and crystal surfaces. Certain 'real world' aspects such as errors in clamping, vibrations, and so on - not included in the SHADOW code at all - of course are left out of consideration.
The energy dependence of the transmission of the photons through the different Be-windows and after mirror reflections is shown In the Fig. 5.15 for the Pt - and in Figs 5.16 and 5.17 for the Si material.

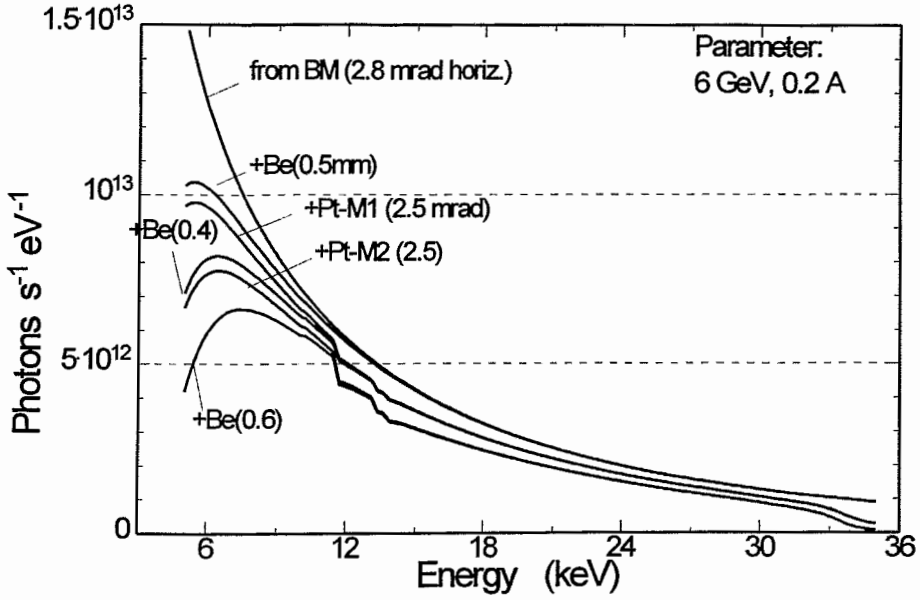

Fig. 5.15: Energy dependence of the transmission of the photons through the Be-Windows (0.5 mm / 0.4 mm / 0.6 mm) and after reflection on the two Pt-coated mirrors at an incidence angle of 2.5 mrad. The number of photons /s/eV was calculated for a bending magnet source (BM) and the following parameter set: 6 GeV, 0.2 A, 2.8 mrad used horizontal divergence, fully accepted vertical divergence

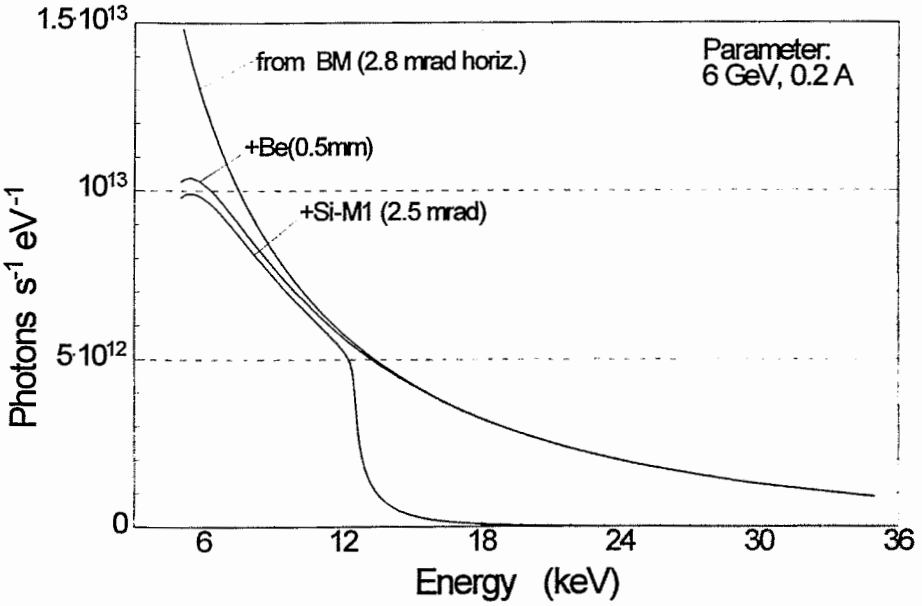

Fig. 5.16: Energy dependence of the transmission of the photons through the front end Be-Window (0.5 mm) and after reflection on the first Si-mirror at an incidence angle of 2.5 mrad. The number of photons /s/eV was calculated for a bending magnet source(BM) and the following parameter set: 6 GeV, 0.2 A, 2.8 mrad used horizontal divergence, fully accepted vertical divergence.

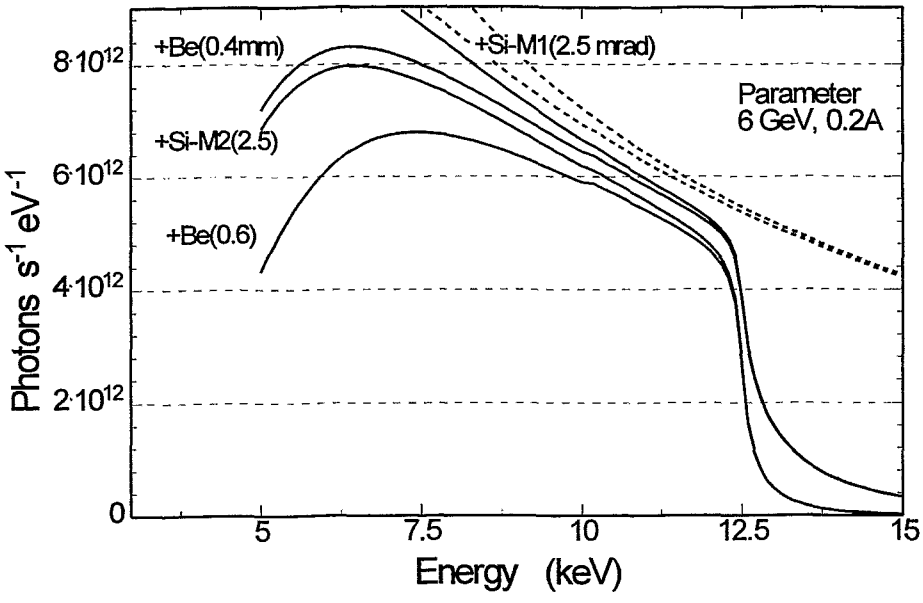

Fig.5.17: Energy dependence of the transmission of the photons through the Be-Window (0.4 mm / 0.6 mm) and after reflection on the two Si-mirrors at an incidence angle of 2.5 mrad. The number of photons /s/eV was calculated for a ESRF bending magnet source (BM) with the parameter set: 6 GeV, 0.2 A, $\Delta\varphi$ =2.8 mrad used horizontal divergence, fully accepted vertical divergence.

5.3.2. Photon Flux at the Image Plane

At the tracing of the rays through the optical system - consisting of optical elements as mirrors, crystals[1], slits, and screens - due to geometrical ray limitations and energy dependent absorption processes a part of the rays is lost. The number of the geometrically as well as energetically 'good' rays of the generated distribution is determined by the geometrical configuration (for instance the limited extensions of the optical elements) as well as by the transmission band width ΔE (FWHM value) of the monochromator. In the simulations the transmitted intensity I_T is represented by the sum number of these 'good' rays after integration over the relevant energy range.
Up to a number N_{ray} ($\leq$5000) the routine SOURCE randomly generates rays with energy values within a preselected energy range $E \pm \Delta E_{ray}/2$.

The transmission factor

$$T_{1eV} \text{ is } T_{1eV} = (I_T / \Delta E) / (N_{ray} / \Delta E_{ray}), \qquad (5.6)$$

and the number of photons / sec at the sample N_{exp} follows than as

[1] In the SHADOW code crystals are not introduced as separate optical units. They are taken into account only as specified mirrors.

$$N_{exp} = N'_{src,1eV} * T_{1eV} * \Delta E . \qquad (5.7)$$

At the ray tracing the (limited) geometrical extensions of the two mirrors M1 and M2 were taken into account. In the Figs. 5.18 for Si(311) and Si(111),respectively, the roughly estimated specified photon flux at the image plane N_{exp} is shown in dependence on energy for the Pt- and Si-mirror configuration as well.

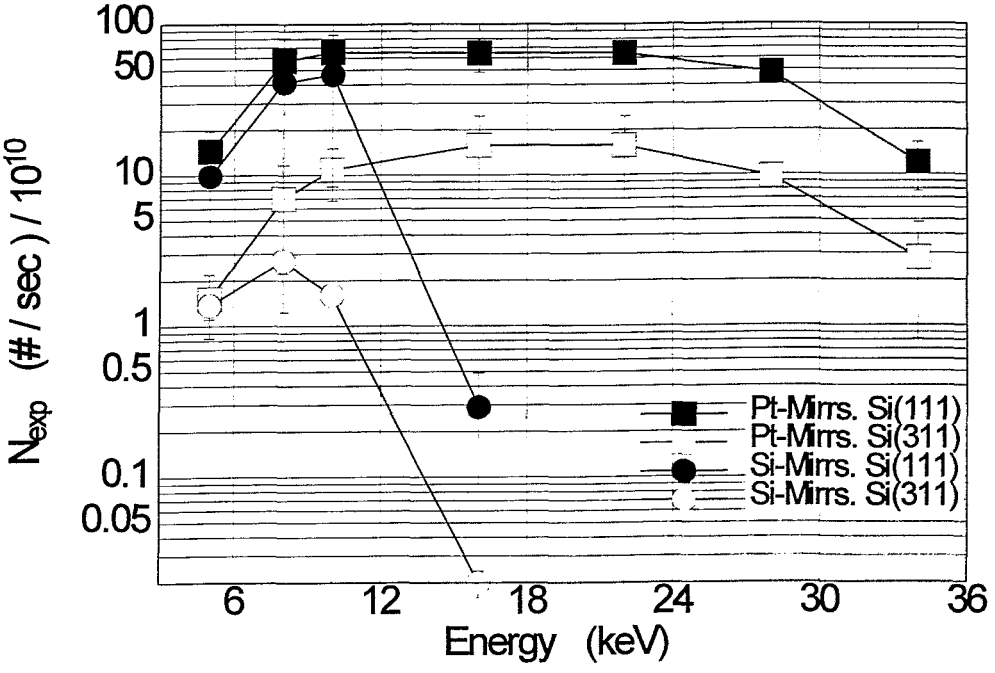

Fig. 5.18: Shadow simulated photon flux at the image plane *behind* a Be-window thickness of 1.3 mm . (Configuration: ESRF BM for 200 mA current and $\Delta\varphi$ =2.8 mrad horizontal divergence. The different monochromator crystals Si(311) and Si(111), respectively, and the different Pt- and Si-mirrors (incidence angle 2.5 mrad in both cases) are indicated by the various symbols.

6. Beamline Vacuum System

6.1. Demands for the Vacuum

The vacuum system for the beamline optics is designed to operate under UHV conditions. The standard vacuum vessels are specified for $5x10^{-9}$ mbar and leak rates better than 10^{-9} mbarl/s. For the mirror vessels a vacuum of 10^{-9} mbar is required. In contrast the vacuum demands for the monochromaor vessel are relaxed to $<10^{-6}$ mbar and a leak rate of $5x10^{-6}$ mbarl/s. The relaxation of the specification was made with respect to the requirement of opening of the vessel for maintenance. To guarantee better vacuum conditions in the other vessels up- and down-streams the monochromator there are beryllium windows inserted for separation (c.f. 4.6.5.).

The hydrocarbon-free vacuum will be achieved by turbomolecular pumps in the HV-region and by ion pumps in the UHV-region.

The vacuum vessels will be made from stainless steel of 304L or 316L grade. For copper parts OHFC quality is required.

Generally, the connections will be performed by conflat flanges. All flange holes are to lie off the center line. The leak test grooves are placed underneath the flange. The exceptions are the opening of the double crystal monochromator vessel the rectangular openings of the mirror vessels. The latter are foreseen for the toploading of the mirrors.

All vacuum vessels and vacuum components should be baked out up to 200°C in order to achieve stable UHV operation.

For the procedures of welding, cleaning and bake out the standard procedures established by the ESRF [6.1] are taken as recommendation.

6.2. The Vacuum Scheme

In the appendix the full vacuum scheme of ROBL is shown. All optical components are also indicated. Additionally to the components described in paragraph 4 there are valves, gauges and pumps integrated. The vacuum system is devided in sections which can be pumped separately. The vacuum interlock system will be built according to the ESRF standard.

In the experimental hutches there are alternative arrangements possible. In the radiochemistry hutch the vacuum tube is interrupted for the normal experimental conditions. Both tube ends are closed with beryllium windows. The glove box is fully separated from the vacuum tubes. When the materials science experiment will be run, the glove box is moved sidewards and the vacuum tube in the radiochemistry hutch is closed in order to reduce absorption by air scattering. If the materials science experiment needs low energy synchrotron radiation then the beryllium windows in the radiochemistry hutch can also be removed (cf. 4.6.4.).
In the radiochemistry hutch there are located two valves each in front of and behind the glovebox. One of each pair belongs to the normal vacuum scheme

and will be operated if any vacuum manipulation is required. The second valve of each pair belongs to the internal safety system of the radiochemistry hutch. It will be operated from the contamination control in the glove box. If there might be an air contamination in the glovebox above a pre-set level an alarm will be given and the safety valves will be closed automatically. This serves to prevent any possible contamination outside the radiochemistry hutch passing through the vacuum tube. The valves will be closed from the glovebox monitoring since this is the first place where contamination can occur.

In the materials science hutch the normal experimental set-up is with the goniometer. The beam will travel its last path in air. The installation of a helium filled tube bringing the beam close to the sample in order to reduce air scattering will be possible. The other possibility is the direct connection of a vacuum chamber for the sample with the vacuum of the beam tube.

7. Concluding Remarks

This documents was written as a final design report for the ROBL project. It covers only the general layout, optics and vacuum system, i.e. the "hard ware" necessary to bring a X-ray beam of definite energy and size from the source to the samples. The intention was to give an overview for ROBL and to discuss the main ideas for the decision towards the adopted design. The main calculations for the optics were presented in order to show which quality of X-ray beams can be expected for the experiments.
The detailed description of the experimental end-stations themselves is the topic of another document.

Acknowledgement

During the design phase and the specification of the equipment for the ROBL project at the ESRF we were supported by many colleagues from the ESRF and the CRGs.
The most extensive help was given to us by Phil Pattison (University of Lausanne) working for the Swiss-Norwegian Beam Line (SNBL CRG) and by Ian Kilvington, the CRG Liason Engineer of the ESRF. We learned very much from the discussions in the CRG Club and are gratefull to all members for advise, especially to Michel Belakhovky (IF CRG) the former club secretary.
Many people from the ESRF have shared their experience with us or gave advise in special questions. As representatives we acknowledge the continous support of M. Hagelstein, E. Bräuer, A. Freund, P. Mackrill, P. Berkvens.
In the Forschungszentrum Rossendorf many colleagues are involved in different aspects of the whole project. We acknowledge discussions with and the support from L. Baraniak, M. Betzl, V. Brendler, M.A. Denecke, S. Dienel, H. Funke, G. Hüttig, H. Krug, W. Möller, W. Neumann, H. Nitsche, W. Oehme, D. Pröhl, T. Reich, P. Reichel, J. Stefan in different stages of the project.

References

[1.1] W. Matz, H. Nitsche, L. Baraniak, G. Bernhard, M. Betzl, V. Brendler, F. Eichhorn, G. Hüttig, K. Leege, P. Merker, W. Möller, D. Pröhl, F. Prokert, P. Reichel, R. Schlenk, J. Steffen, Conceptual Design Report: A Beamline for Radiochemistry and Ion Beam Physics on a Bending Magnet Source at the ESRF (Project ROBL), internal report, FZR/ROBL 05/94, Rossendorf, March 1994

[3.1] ESRF, Beamline Handbook editions. 1994, 1995, Grenoble (see also WWW: http//www.esrf.fr)

[4.1] Ph. Coppens, Synchrotron X-ray Crystallography, Academic Press, London 1992, appendixes B and C
[4.2] ESRF Foundation Phase Report (Red Book), Grenoble, February 1987
[4.3] ESRF Annual Report 1993, ed. Y. Petroff, p.4, Grenoble 1994
[4.4] G.K. Green, Spectra and Optics of Synchrotron Radiation, Brookhaven National Laboratory, Upton, New York, 1976
[4.5] B.W. Batterman, D.H. Bilderback, in: Handbook of Synchrotron Radiation, vol 3, ch. 4, North-Holland, Amsterdam 1983
[4.6] S. Krinsky, M.L. Perlman, and R.E. Watson, in: Handbook of Synchrotron Radiation, vol 1A, ch. 2, North-Holland, Amsterdam 1983
[4.7] F. Prokert, X-ray mirrors for ROBL, internal report ROBL 08/94, Rossendorf 1994
[4.8] F. Prokert, Ray tracing calculations for ROBL using the SHADOW code, internal report ROBL 11/95, Rossendorf 1995
[4.9] Ph. Coppens, Synchrotron X-ray Crystallography, Academic Press, London 1992, ch. 3
[4.10] ESRF Beamline Handbook, ed. 1994, p.10, ESRF, Grenoble,
[4.11] T. Mairs (ESRF, machine group) private communication

[5.1] B. Lai and F. Cerrina, *SHADOW: A Synchrotron Ray-Tracing Program*; Nucl .Instr. & Methods **A246**, 337 (1986)
[5.2] B.Lai, K. Chapman, P. Runkle, and F. Cerrina, Rev. Sci. Instrum. **60**, 2127 (1989)
[5.3] M. Sanchez del Rio, *Running SHADOW under UNIX at ESRF,* EXP/MSR/91 October 1992; *The very basic of SHADOW,* MSR 93/06/01 (internal ESRF Documentations)
[5.4] C.J. Sparks, Jr., B.S. Borie, and J.B. Hastings, Nucl. Instr. & Methods **172**, 273 - 242 (1980)
[5.5] G.K. Green, *Spectra and Optics of Synchrotron Radiation* Brookhaven National Laboratory, Upton, New York (1976)

[6.1] Welding Requirements; General Cleaning Procedure for Stainless Steel Vacuum Components; Bakeout and Outgassing Procedure for Vacuum Vessels ESRF/ENG/89/07/B; ESRF/VAC/ 88-09/B; ESRF/VAC 90-02 Internal documents of the ESRF, Grenoble

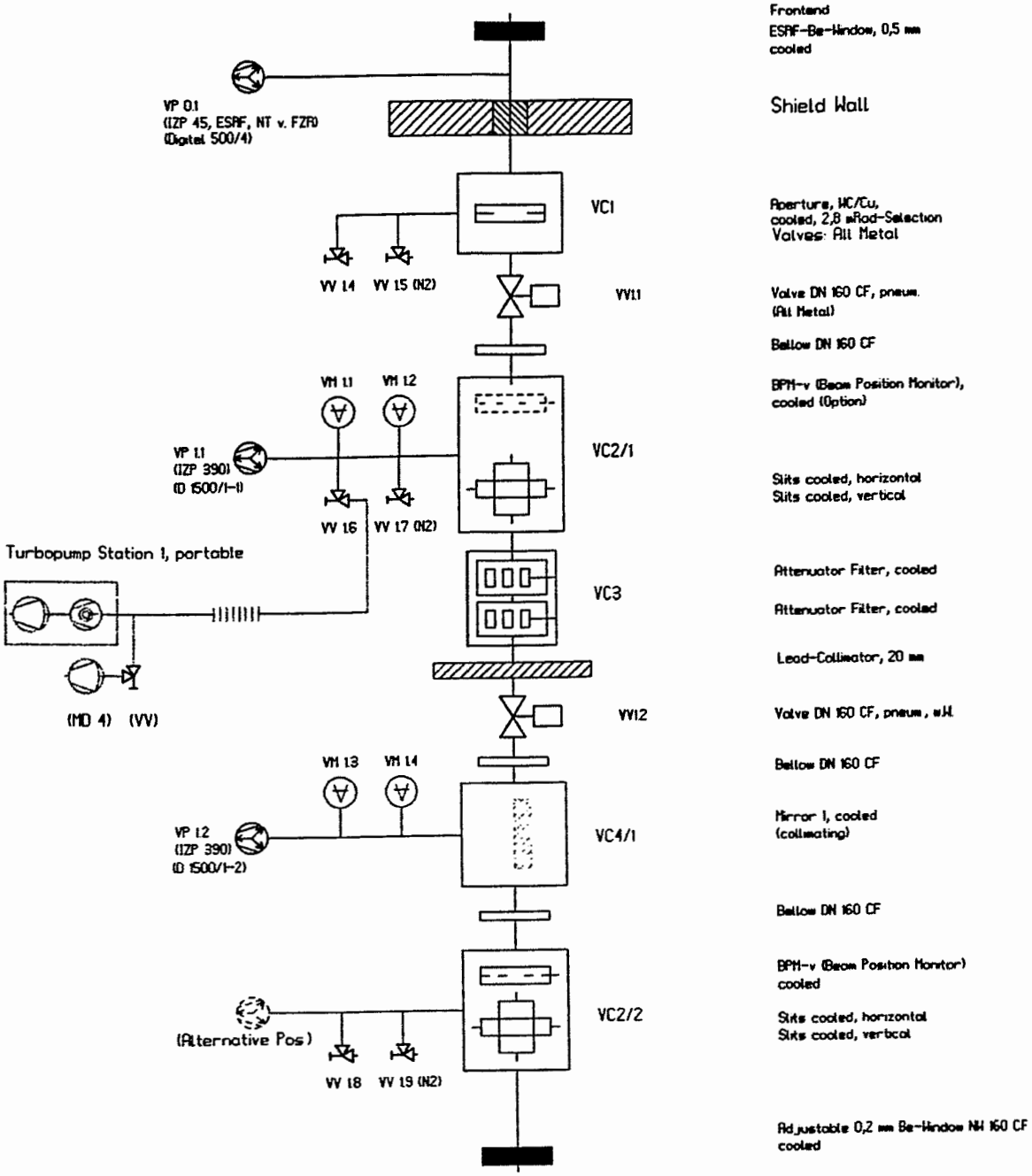

Appendix 1: Scheme of vacuum system and beamline components of ROBL
1: Optics hutch first part

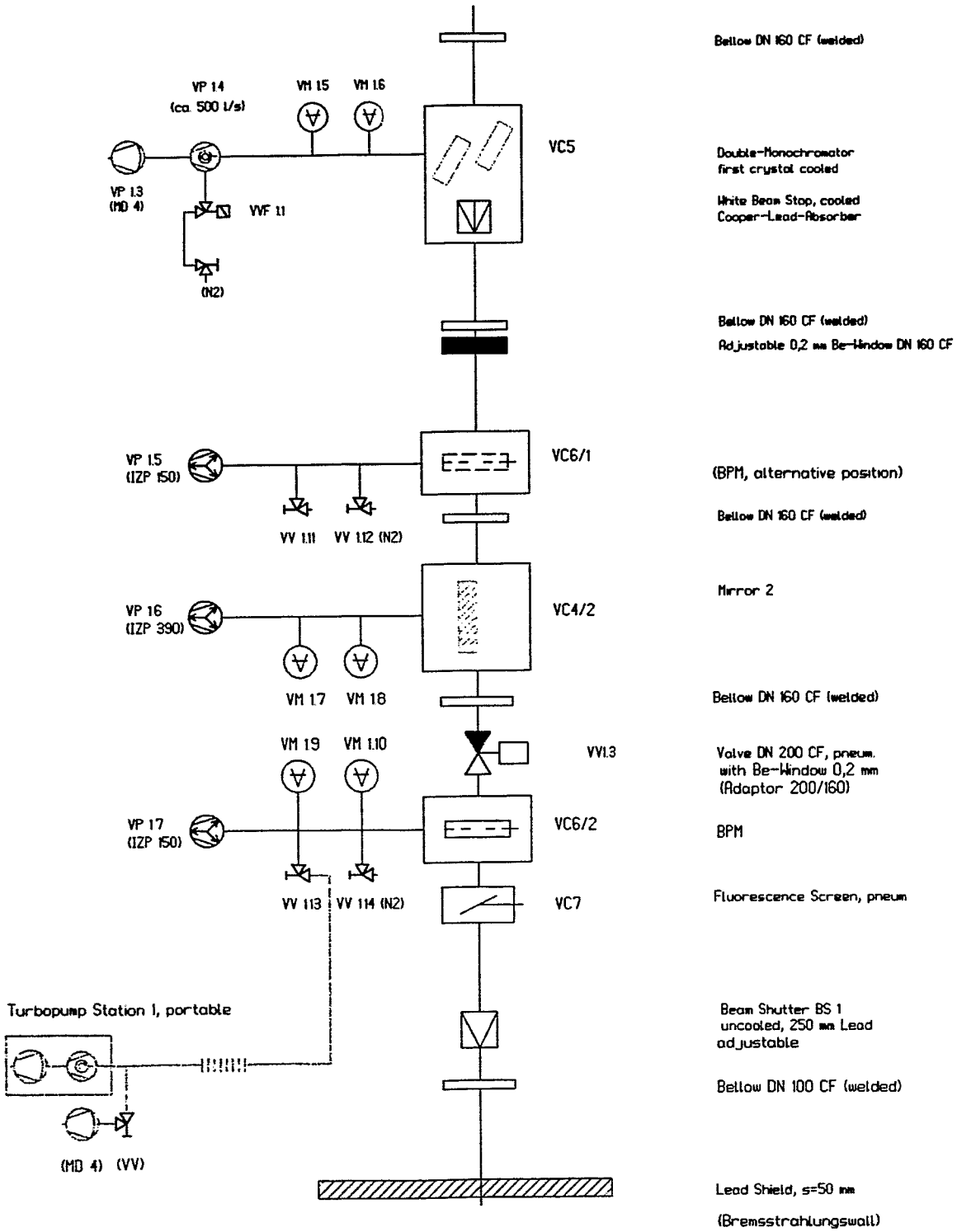

Appendix 1: Scheme of vacuum system and beamline components of ROBL
2: Optics hutch second part

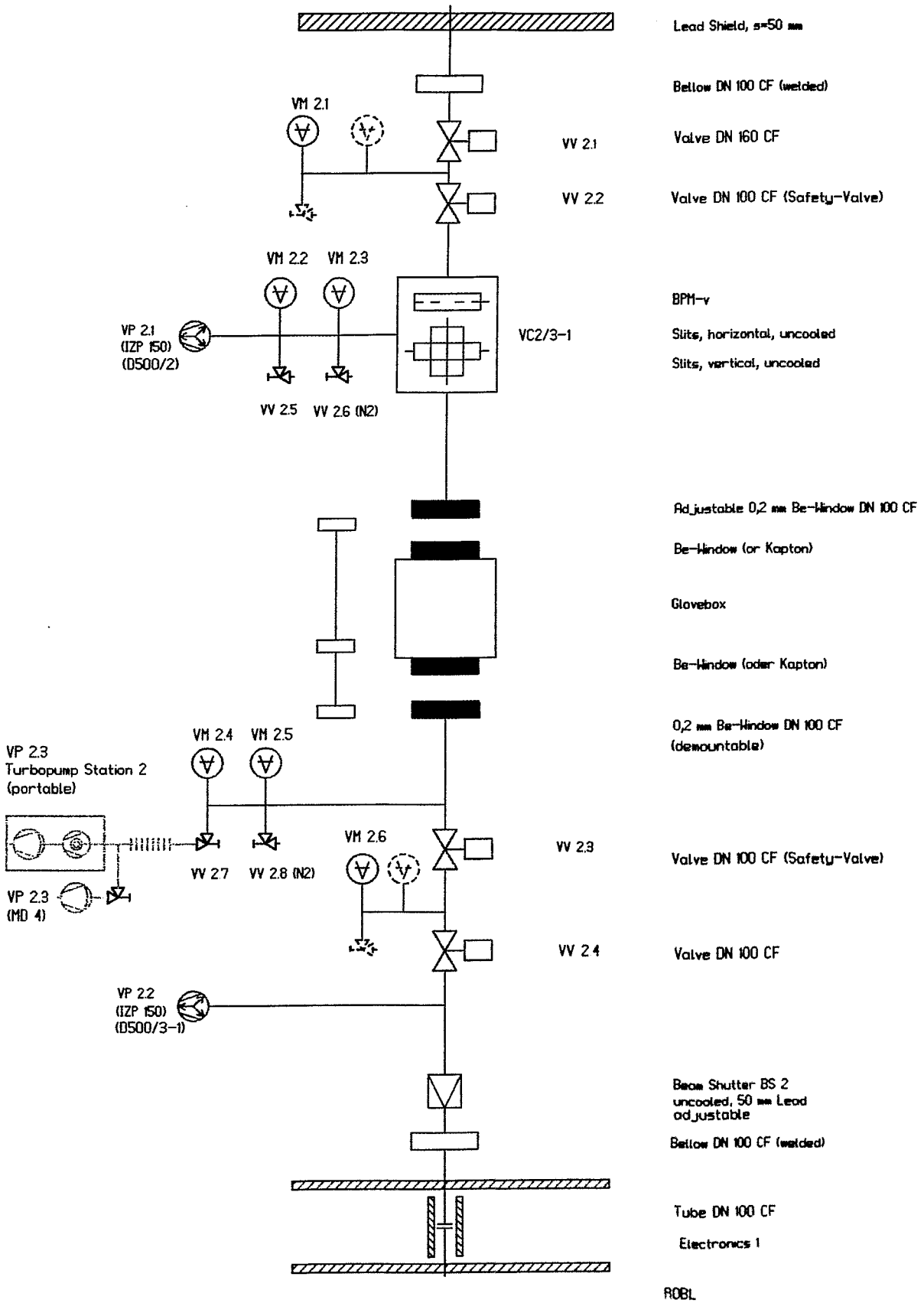

Appendix 1: Scheme of vacuum system and beamline components of ROBL 3: Radiochemistry hutch

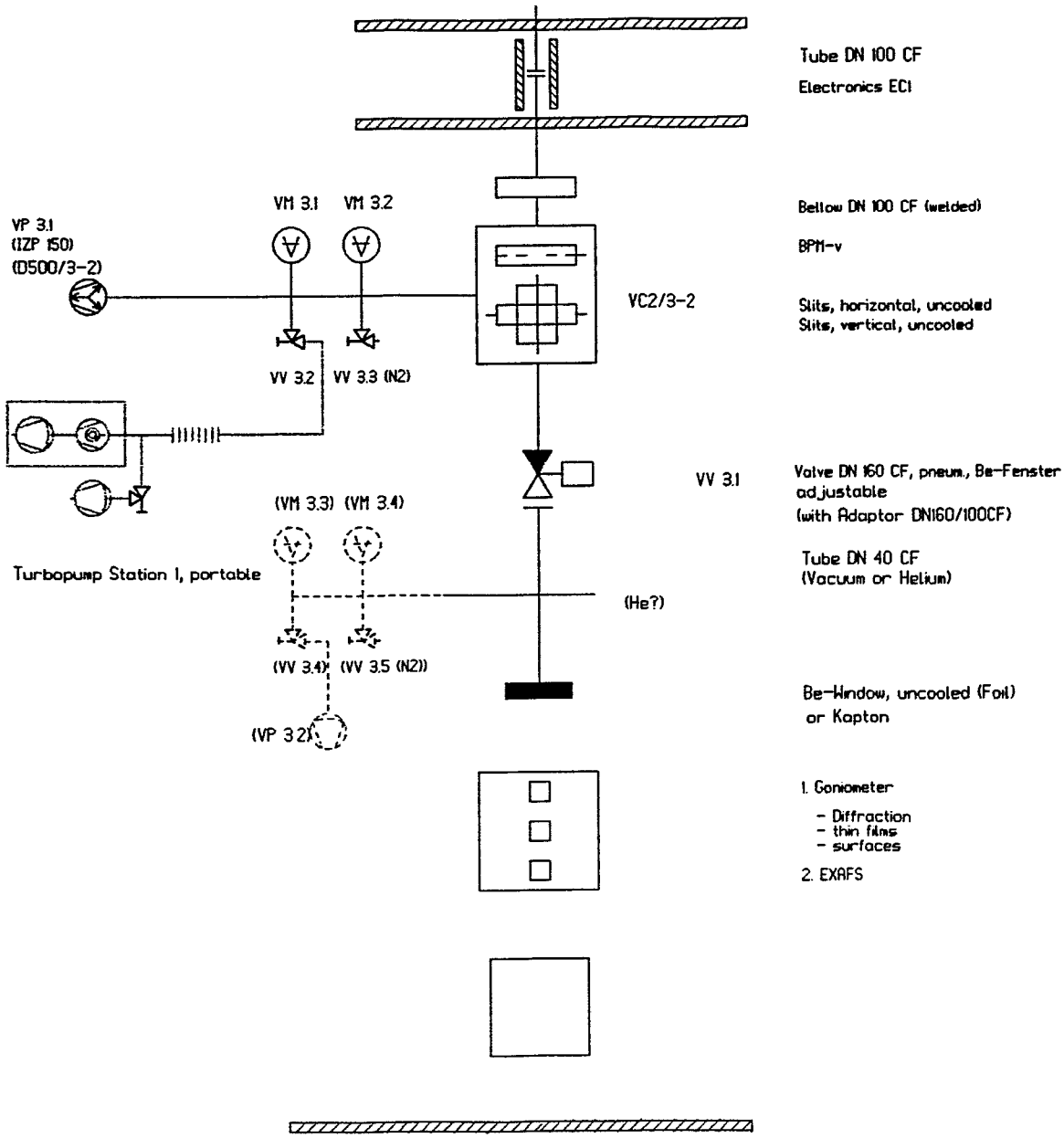

Appendix 1: Scheme of vacuum system and beamline components of ROBL 4: Materials science hutch